

CHARACTERIZATION OF *Mycobacterium tuberculosis* CmtR<sup>Mtb</sup>, A Pb<sup>II</sup>/Cd<sup>II</sup>-  
SENSING SmtB/ArsR METALLOREGULATORY REPRESSOR, AND A  
HOMOLOG FROM *Streptomyces coelicolor* A3(2)

A Thesis

by

YUN WANG

Submitted to the Office of Graduate Studies of  
Texas A&M University  
in partial fulfillment of the requirements for the degree of

MASTER OF SCIENCE

August 2005

Major Subject: Biochemistry

CHARACTERIZATION OF *Mycobacterium tuberculosis* CmtR<sup>Mtb</sup>, A Pb<sup>II</sup>/Cd<sup>II</sup>-  
SENSING SmtB/ArsR METALLOREGULATORY REPRESSOR, AND A  
HOMOLOG FROM *Streptomyces coelicolor* A3(2)

A Thesis

by

YUN WANG

Submitted to the Office of Graduate Studies of  
Texas A&M University  
in partial fulfillment of the requirements for the degree of

MASTER OF SCIENCE

Approved by:

Chair of Committee,	David P. Giedroc
Committee Members,	David O. Peterson
	Paul A. Lindahl
	J. Martin Scholtz
Head of Department,	Gregory D. Reinhart

August 2005

Major Subject: Biochemistry

## ABSTRACT

Characterization of *Mycobacterium tuberculosis* CmtR<sup>Mtb</sup>, a Pb<sup>II</sup>/Cd<sup>II</sup>-sensing SmtB/ArsR Metalloregulatory Repressor, and a Homolog from *Streptomyces. coelicolor* A3(2).

(August 2005)

Yun Wang, B.S., Fudan University

Chair of Advisory Committee: Dr. David P. Giedroc

The SmtB/ArsR family of prokaryotic metalloregulators are winged-helix transcriptional repressors that collectively provide resistance to a wide range of both biologically required and toxic heavy metal ions. CmtR<sup>Mtb</sup> is a recently described Cd<sup>II</sup>/Pb<sup>II</sup> regulator expressed in *M. tuberculosis* that is structurally distinct from the well-characterized SmtB/ArsR Cd<sup>II</sup>/Pb<sup>II</sup> sensor, *S. aureus* plasmid pI258-encoded CadC. From functional analyses and a multiple sequence alignment of CmtR homologs, CmtR<sup>Mtb</sup> is proposed to bind Pb<sup>II</sup> and Cd<sup>II</sup> via coordination by Cys57, Cys61 and Cys102 [Cavet *et al.* (2003) *J. Biol. Chem.* **278**, 44560-44566]. To better understand the mechanism how CmtR<sup>Mtb</sup> utilizes specific metal ions to perform transcriptional repressor function, both CmtR<sup>Mtb</sup> and its homolog in *S. coelicolor* A3(2) (CmtR<sup>Sc</sup>) were studied. We establish here that both wild-type and C102S CmtR<sup>Mtb</sup> are homodimers and bind Cd<sup>II</sup> and Pb<sup>II</sup> via formation of cysteine thiolate-rich coordination bonds. UV-Vis optical spectroscopy and <sup>113</sup>Cd NMR spectroscopy ( $\delta=480$  ppm) suggest two or three thiolate donors, while <sup>111m</sup>Cd perturbed angular correlation (PAC) spectroscopy establish an unusual trigonal pyramidal coordination geometry. C102S CmtR<sup>Mtb</sup> binds Cd<sup>II</sup> and Zn<sup>II</sup> with only  $\approx 10$ -20

fold lower affinity relative to wild-type CmtR<sup>Mtb</sup>, but  $\approx$  100-1000-fold lower for Pb<sup>II</sup>. Quantitative investigation of CmtR-*cmt* O/P binding equilibria using fluorescence anisotropy reveals that Cys57 and Cys61 anchor the coordination complex with Cys102 functioning as a key allosteric ligand, while playing only an accessory role in stabilizing the metal complex in the free protein. Similar metal titration experiments were carried out with a putative CmtR homolog from *S. coelicolor* A3(2) (CmtR<sup>Sc</sup>) and a double cysteine substitution mutant C110G/C111S CmtR<sup>Sc</sup>. The implications of these findings on the evolution of distinct metal sensing sites in a family of homologous proteins are discussed.

## ACKNOWLEDGMENTS

I am indebted to Dr. Giedroc for his patient guidance, powerful support and enthusiastic encouragement during my graduate studies. I would also like to thank the members of my committee, Dr David O. Peterson, Dr J. Martin Scholtz and Dr Paul A. Lindahl for their time and useful suggestions. I am grateful to my colleagues in Giedroc Lab, especially Dr Xiaohua Chen, Dr Tong Liu, Dr Mario Pennella and Mr Peter Cornish, who shared their valuable experience with me and gave me much guidance. Without their help, I would not have been able to grow from one with green hand to obtain the data in this thesis so quickly.

## TABLE OF CONTENTS

	Page
ABSTRACT.....	iii
ACKNOWLEDGMENTS.....	v
TABLE OF CONTENTS.....	vi
LIST OF FIGURES.....	viii
LIST OF TABLES.....	x
CHAPTER	
I INTRODUCTION.....	1
II MATERIALS AND METHODS.....	12
Materials.....	12
Methods.....	12
III FUNCTIONAL CHARACTERIZATION OF <i>M. tuberculosis</i> CmtR VARIANTS: Cys102 IS A KEY METAL LIGAND IN ALLOSTERIC REGULATION BUT IN METAL CHELATES STABILIZATION.....	15
Introduction.....	15
Experimental procedures.....	18
Results.....	23
Discussions.....	44
Conclusion.....	52
IV METAL BINDING PROPERTIES OF A PUTATIVE CmtR HOMOLOG ENCODED BY <i>S. coelicolor</i> A(3)2.....	54
Introduction.....	54
Experimental procedures.....	59
Results and discussions.....	60
V SUMMARY AND PERSPECTIVE.....	68

REFERENCES.....	72
VITA.....	80

## LIST OF FIGURES

FIGURE	Page
1 Metal resistance operons regulated by SmtB/ArsR family transcriptional repressors.....	3
2 Summary of metal binding sites and thermodynamic parameters of SmtB/ArsR proteins.....	5
3 Structure of cyanobacterial apo SmtB.....	7
4 Structure of <i>S. aureus</i> pI258 CadC.....	9
5 (A) Homology model of the CmtR homodimer based on the crystal structure of apo-SmtB (B) Two windows derived from multiple sequence alignment of <i>M. tuberculosis</i> CmtR <sup>Mtb</sup> and putative homologs.....	17
6 Analytical sedimentation equilibrium ultracentrifugation of (A) apo-wild type CmtR <sup>Mtb</sup> and (B) apo-C102S CmtR <sup>Mtb</sup> .....	24
7 Representative anaerobic Cd <sup>II</sup> titrations of (A) apo wild-type CmtR <sup>Mtb</sup> and (B) apo C102S CmtR <sup>Mtb</sup> .....	25
8 Representative Cd <sup>II</sup> competition assays carried out with (A) wild-type CmtR <sup>Mtb</sup> and (B) C102S CmtR <sup>Mtb</sup> in presence of 227 $\mu$ M EDTA.....	27
9 Representative anaerobic Pb <sup>II</sup> titrations of (A) apo wild-type CmtR <sup>Mtb</sup> (B) apo C102S CmtR <sup>Mtb</sup> and (C) apo C102S CmtR <sup>Mtb</sup> and 91.2 $\mu$ M EGTA.....	28
10 Representative titrations of Zn <sup>II</sup> into a mixture of mag-fura-2 and either (A) wild-type CmtR <sup>Mtb</sup> or (B) C102S CmtR <sup>Mtb</sup> .....	32
11 <sup>113</sup> Cd NMR spectrum of <sup>113</sup> Cd-substituted CmtR <sup>Mtb</sup> .....	34
12 <sup>111m</sup> Cd PAC spectra of wild-type (WT) ( <i>top</i> ) and C102S ( <i>bottom</i> ) CmtR <sup>Mtb</sup> .....	37
13 Representative <i>cmt</i> O/P binding by wild-type (A) and C102S (B) CmtR <sup>Mtb</sup> as monitored by fluorescence anisotropy.....	41



FIGURE	Page
14 Sequence comparison of (A) <i>M. tuberculosis</i> CmtR <sup>Mtb</sup> and 2 putative homologs from <i>S. coelicolor</i> A3(2) (B) SCO0875's immediate downstream gene SCO0874 and its homologs generated by Cluster X.....	56
15 Schematic representations of Cmt <sup>Sc</sup> and the putative SCO3521/SCO3522 operons.....	57
16 Apo-subtracted difference spectrum of Cd <sup>II</sup> -saturated (A) apo wild-type CmtR <sup>Sc</sup> (B) apo C110G/C111S CmtR <sup>Sc</sup> (C) Cd <sup>II</sup> -EDTA competition binding isotherm in which 20.9 μM wt CmtR <sup>Sc</sup> was titrated with Cd <sup>II</sup> in presence of 227 μM EDTA.....	61
17 Apo-subtracted difference spectrum of Pb <sup>II</sup> -saturated apo (A) wild-type CmtR <sup>Sc</sup> (B) C110G/C111S CmtR <sup>Sc</sup> .....	65
18 Representative titration of Zn <sup>II</sup> into a mixture of mag-fura-2 and wild-type CmtR <sup>Sc</sup> .....	66

## LIST OF TABLES

TABLE	Page
1 Fitted parameters derived from the $^{111m}\text{Cd}$ perturbed angular correlation spectra obtained for wild-type and C102S CmtR <sup>Mtb</sup> s.....	39
2 Calculated PAC parameters for model coordination complexes derived from the semi-empirical BASIL method.....	40
3 Summary of $K_i$ obtained for the binding of apo, $\text{Cd}^{\text{II}}$ -substituted and $\text{Zn}^{\text{II}}$ -substituted wild-type and C102S CmtR to <i>cmt</i> O/P DNA.....	45

## CHAPTER I

### INTRODUCTION

The first row transition metal ions, including zinc, copper, iron, nickel, manganese and cobalt, play a wide range of biological roles essential for cell survival. Although they are often found at relatively low concentrations, these metal ions can be selectively accumulated by cells. Some metal ions, like Cu and Fe, function as enzyme cofactors under normal physiological conditions, but when present in excess they catalyze cytotoxic reactions via redox chemistry (1). The recent discovery of the genetic basis of Menkes, Wilson and Lou Gehrig's diseases identified the important relationship of these diseases to intracellular metal ion metabolism (2-5). To maintain an intracellular pool of these essential metal ions compatible with cellular needs, all cells, from bacteria to eukaryotic cells, have evolved homeostasis mechanisms that balance the expression of genes that encode proteins involved in specific metal uptake, efflux and sequestration of essential metal ions (6-8). The same regulatory mechanisms are exploited in many cases to provide resistance to heavy metal pollutants, including cadmium, lead, mercury and arsenic (9-11), which are extremely toxic, at moderate intracellular concentration. (1)

Cell membranes are critical components for a cell to perform its biological functions. It is not only a lipid barrier, but also a part of total cellular structure through direct interactions that form the protein network in the cell (12). In order to maintain metal ion homeostasis, the cell membrane needs to prevent metal ions from passively

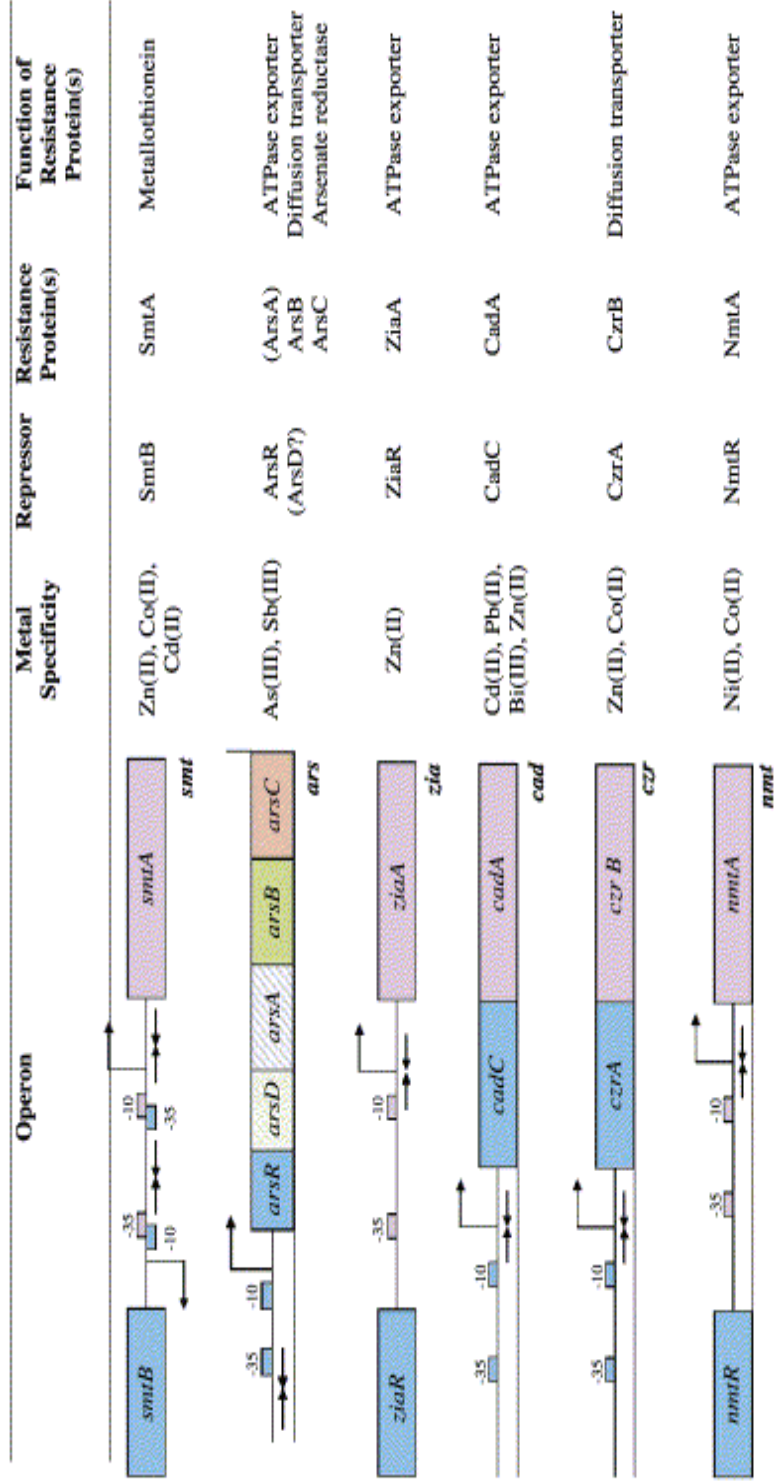
---

This thesis follows the style of *Biochemistry*.

entering the cytosol, but must overcome this protective barrier to allow cell to meet its metal requirements (13). Therefore, under metal-limiting conditions, metal ions and selected chelating complexes are internalized by active transport, while systems for metal sequestration or efflux are induced when metal ions accumulate to excess (13).

Members of the SmtB/ArsR family of prokaryotic metalloregulatory transcriptional repressors regulate intracellular metal ion concentrations under conditions of metal excess by functioning as metalloregulatory sensors (for a recent review, see ref. (10)). These repressors sense di- and multivalent heavy metal ions and regulate the expression of metal regulated operons that typically encode metal-specific efflux pumps, membrane-bound transporters or intracellular chelators, *e.g.*, metallothioneins (10, 14). Figure 1 summarizes metal resistance operons regulated by well-studied SmtB/ArsR family transcriptional repressors. SmtB/ArsR family members appear to act exclusively as transcriptional repressors of metal resistance proteins (10). This contrasts to another class of prokaryotic metal sensors, the paradigm for which is the Hg<sup>II</sup> sensor MerR (15), that become potent transcriptional activators in the presence bound metals (11). Transcription is repressed when the apo-SmtB/ArsR proteins are specifically bound to the operator/promoter (O/P) region (10) and is derepressed upon specific metal binding. Derepression is mediated by typically strong allosteric negative regulation of O/P binding.

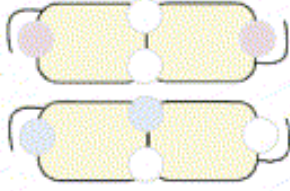
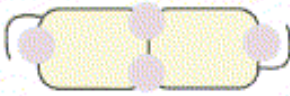

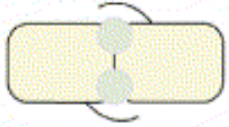
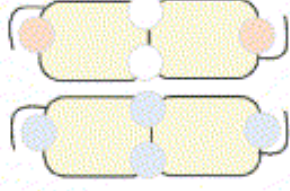
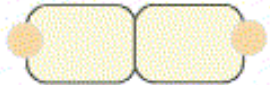
SmtB/ArsR family metal sensors are widely distributed throughout pathogenic and non-pathogenic bacterial and archaeal species, such as archaea, proteobacteria, firmicutes, actinobacteria and cyanobacteria (16). This protein family is enriched in



**FIGURE 1:** Metal resistance operons regulated by SmtB/ArsR family transcriptional repressors. General operon structures which confer metal resistance in bacteria that are regulated *in vivo* by the indicated SmtB/ArsR repressors. Note that not all *ars* operons contain the *arsD* and *arsA* genes. Reproduced with permission from Busenlehner et al, (2003).

some bacterial species, which is considered to be a reflection of a complex life cycle (16). For example, the actinobacterium *Streptomyces coelicolor*, which is characterized by an elaborate life cycle resembling multicellular eukaryotes, encodes 14 SmtB/ArsR family members (16); another actinobacterium *Mycobacterium tuberculosis*, which is a slow-growing pathogen and the causative agent of tuberculosis in humans, encodes 10 SmtB/ArsR regulators (17, 18). Metal sensor-dependent regulation of the transcription of these operons confers resistance to a wide range of heavy metal ions including  $Zn^{II}$  (19),  $Co^{II}$ ,  $Ni^{II}$  (20) and  $Cu^I/Ag^I$  (21), as well as  $Cd^{II}$ ,  $Pb^{II}$  (22),  $Bi^{III}$  (23),  $As^{III}$ , and  $Sb^{III}$  (10, 24).

Because metal binding properties are so important for SmtB/ArsR family protein to execute their functions as transcriptional repressors, it is important to understand the structures of metal sensing sites present and how each differentiates among various metals ions. Previous comparative spectroscopic and functional studies of family members including *Synechococcus* SmtB, *S. aureus* pI258 CadC, *Synechocystis* ZiaR, *S. aureus* CzrA and *M. tuberculosis* NmtR have identified two distinct metal binding sites within the homodimeric repressor (20, 25-29). One is designated as  $\alpha 3N$  (or  $\alpha 3$  for ArsR) and the other is named as  $\alpha 5$  (or  $\alpha 5c$  for NmtR) metal binding sites (10). A typical  $\alpha 3N$  site is composed of three or four cysteine thiolate ligands while  $\alpha 5$  site consists of four metal binding ligands derived exclusively from the C-terminal  $\alpha 5$  helices. pI258 CadC is a representative of  $\alpha 3N$  site containing proteins, while SmtB and CzrA are representative members that contain  $\alpha 5$  site (10). Figure 2 summarizes the metal binding sites in selected SmtB/ArsR family proteins.

Repressor	Metal Binding Sites	Metals	Regulatory Site
	$\alpha$ 3N $\alpha$ 5's $\alpha$ 3N		
SmtB <sup>a</sup>		Zn(II) Co(II)	$\alpha$ 5
ZiaR <sup>b</sup>		Zn(II)	$\alpha$ 5 and $\alpha$ 3N?
CzrA <sup>c</sup>		Co(II) Zn(II)	$\alpha$ 5
NmtR <sup>d</sup>		Ni(II) Co(II)	$\alpha$ 5C
CadC <sup>e</sup>		Cd(II) Pb(II) Bi(III) Zn(II) Co(II)	$\alpha$ 3N
ArsR <sup>f</sup>		As(III) Sb(III)	$\alpha$ 3

**FIGURE 2:** Summary of metal binding sites and thermodynamic parameters of SmtB/ArsR proteins. Cartoon representations of functionally characterized SmtB/ArsR repressors depicting a ‘theme and variations’ model for metal binding (<sup>a</sup>(25, 26, 28); <sup>b</sup>(28); <sup>c</sup>(30); <sup>d</sup>(20, 27); <sup>e</sup>(22, 31); <sup>f</sup>(32, 33)). Metal ions, denoted as spheres, are color-coded: blue-Co<sup>II</sup>; purple-Zn<sup>II</sup>; green-Ni<sup>II</sup>; pink-Cd<sup>II</sup>/Pb<sup>II</sup>; orange-As<sup>III</sup>. Adapted from Busenlehner et al, (2003).

Recent advances in x-ray crystallography have provided detailed insight as to the structural basis of metal binding in SmtB/ArsR proteins. Available crystal structures of this family proteins all reveal stable homodimers with a *winged* helix-turn-helix DNA binding motif, which is a distinctive feature of SmtB/ArsR sensors (30, 34, 35). This HTH (helix-turn-helix) motif can be found in basal and specific transcription factors from archaea, protokaryotes to eukaryotes and is probably one of the most ancient conserved features of transcriptional apparatus (36). The *winged* HTH (wHTH) superclass includes the majority of prokaryotic transcription factors, which are characterized by presence of a C-terminal  $\alpha$ -hairpin unit (the wing) that packs against the shallow cleft of the partially open tri-helical core (36-38). There are thirteen major protein families that possess prokaryotic wHTH domains with the SmtB/ArsR family comprising the largest protein sequences that are thought to derive from a common evolutionary ancestor (36). These protein families can be found in both archaea and bacteria with distinct pan-archaeal and pan-bacterial branches within them, which suggests they belong to an ancestral core that is the universal common ancestor of all extant life forms (36).

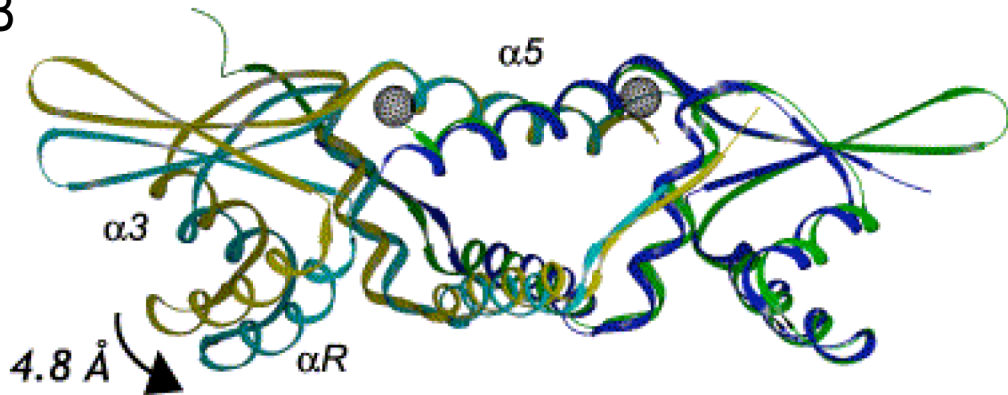
In 1998, the first x-ray crystallographic structure SmtB/ArsR protein was reported (35). This was the cyanobacterial SmtB, the regulator of the Smt (*Synechococcus* metallothionein) gene, ie, apo-SmtB. More recently, the Giedroc and Sacchettini groups solved the structures of apo-SmtB to higher resolution as well as the structure of  $Zn_1$ ,  $Zn_2$ -SmtB and apo,  $Zn_2$  forms of the related  $Zn^{II}/Co^{II}$  sensor *Staphylococcus aureus* CzrA (30). From a comparison of their structures, Eicken et al



A



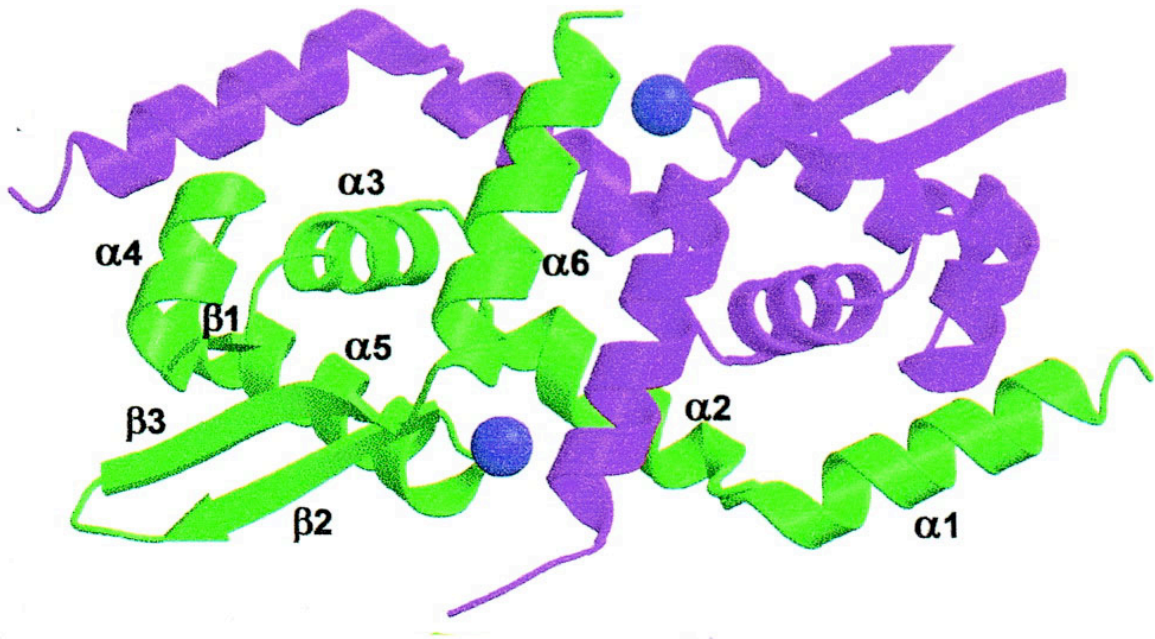
B



**FIGURE 3:** Structure of cyanobacterial SmtB. (A) Sequence alignment of *Synechococcus* SmtB and *S. aureus* CzrA, (B) Superposition of apo-SmtB (green and gold-colored protomers) with Zn<sub>2</sub> α5-SmtB (blue and cyan-colored subunits), the latter solved to 2.3 Å resolution. The Figure was generated by performing a superposition of the C atoms of the α5 helices of the green- and blue-shaded subunits of apo- and Zn<sub>2</sub> α5-SmtB, respectively. Figures were created using SPOCK: <http://mackerel.tamu.edu/spock> Adapted from Eicken et al, (2003)

hypothesized that Zn<sup>II</sup> binding to the  $\alpha$ 5 site drives a quaternary structural switch that is mediated by direct hydrogen bonding of a nonliganding face of a coordinating histidine (N $\epsilon$ 2 of His117 in SmtB) to a backbone carbonyl oxygen (Arg87') found in the turn region between the  $\alpha$ 4 helix and the  $\beta$ -hairpin of the opposite subunit (Figure 3B). Each SmtB monomer consists of five  $\alpha$ -helices and two  $\beta$ -strands arranged into an  $\alpha$ 1- $\alpha$ 2- $\alpha$ 3- $\alpha$ R- $\beta$ 1- $\beta$ 2- $\alpha$ 5-fold, with  $\alpha$ 3-turn- $\alpha$ R forming a standard helix-turn-helix motif (10, 30, 35) (Figure 3A). Two zinc ions were bound to the interhelical  $\alpha$ 5 metal-binding sites which straddled the dimer interface formed by two  $\alpha$ 5 helices, which is called  $\alpha$ 5 site (30). Upon Zn<sup>II</sup> binding to SmtB, there is a large movement of the HTH and  $\beta$ -wings of one subunit relative to the other. (30) (Figure 3). The overall structural compaction induced by metal binding can alter the positions of  $\alpha$ R helix (30). Although *S. aureus* CzrA contains the same  $\alpha$ 5 metal binding site as SmtB, the metal ion appeared to induce little or no structural changes compared to SmtB (30).

The best characterized Cd<sup>II</sup>/Pb<sup>II</sup> sensor in SmtB/ArsR family is *Staphylococcus aureus* pI258-encoded CadC, which regulates the expression of a P<sub>1B</sub>-type ATPase metal efflux pump, CadA. In CadCs and other closely related thiophilic metal sensors, metals bind to an  $\alpha$ 3N site that adopts a trigonal or distorted tetrahedral geometry, formed by three invariant Cys ligands, one from the N-terminal unstructured region (a fourth conserved Cys is often found here as well) and two derived from a ..CVC.. sequence in the putative  $\alpha$ 3 helix (22, 23, 29, 39, 40). pI258 CadC binds Cd<sup>II</sup> and Pb<sup>II</sup> to the  $\alpha$ 3N site that is necessary and sufficient for metalloreulation of the *cad* O/P binding (29). In contrast, the C-terminal  $\alpha$ 5 helix donates a mixture of carboxylate and imidazole ligands



**FIGURE 4:** Structure of *S. aureus* pI 258 CadC. Ribbon diagram of the CadC dimer with secondary structural units (N- $\alpha 1$ - $\alpha 2$ - $\alpha 3$ - $\beta 1$ - $\alpha 4$ - $\alpha 5$ - $\beta 2$ - $\beta 3$ - $\alpha 6$ -C). The two zinc ions are shown as blue spheres. Adapted from Ye et al, (2005)

to a pair of symmetry- related  $\alpha 5$  sites, that form tetrahedral complexes in the  $Zn^{II}$  sensors SmtB and CzrA, and octahedral coordination complexes in  $Ni^{II}$  sensor *M. tuberculosis* NmtR (19, 25, 27).

A recently reported x-ray crystal structure of *Staphylococcus aureus* pI258 CadC at 1.9 Å resolution provide direct structural evidence for the existence of both  $\alpha 3N$  and  $\alpha 5$  metal binding sites, projected previously on the basis of absorption spectroscopy (20, 27, 29) (Figure 4) (34). The  $\alpha 3N$  site was proposed to constituted by Cys7, Cys11, Cys58 and Cys60 (29). The structure reveals that this site is likely formed by Cys7/11 from the  $\alpha 1$  helix (corresponding to an  $\alpha$ -helices immediately preceding the  $\alpha 1$  helix of SmtB/CzrA) of one monomer and Cys58/60 pair from the  $\alpha 4'$  (corresponding to  $\alpha 3'$  helix in SmtB/CzrA) helix of the other monomer (34). The  $\alpha 5$  site is formed between the  $\alpha 6$  and  $\alpha 6'$  helices of the dimerization interface ( $\alpha 6$  corresponds to the  $\alpha 5$  helix in SmtB/CzrA) (34). The formation of this site involves in Asp101 and His103 from one monomer and His114', Glu117' from the other monomer (34), exactly as predicted (29). Since CadC possesses two distinct metal binding sites ( $\alpha 3N$  and  $\alpha 5$ ) but only one ( $\alpha 3N$ ) is required for metalloregulation (29, 34), it has been hypothesized that pI258 CadC is an evolutionary intermediate between ArsR ( $\alpha 3$ ) and SmtB ( $\alpha 5$ ) (34).

*Mycobacterium tuberculosis* H37Rv CmtR (CmR<sup>Mtb</sup>) is a  $Pb^{II}/Cd^{II}$ -specific SmtB/ArsR sensor discovered in 2003 (18). It is the second SmtB/ArsR family member characterized in this organism following the discovery of  $Ni^{II}/Co^{II}$  sensor NmtR in 2002 (27). CmR<sup>Mtb</sup> is structurally distinct from the paradigm  $Pb^{II}/Cd^{II}$  -specific sensor pI258

CadC discussed above, since it lacks both  $\alpha 3N$  and  $\alpha 5$  metal sites and therefore possesses novel metal sensing sites (39). Previous *in vivo*  $\beta$ -galactosidase assays carried out in *M. smegmatis* revealed that *M. tuberculosis H37Rv* CmtR<sup>Mtb</sup> was capable of metalloregulating reporter gene expression in response to Cd<sup>II</sup> and Pb<sup>II</sup> salts, but interestingly, not Zn<sup>II</sup>, a surprising property that also distinguishes CmtR<sup>Mtb</sup> from other Cd<sup>II</sup>/Pb<sup>II</sup> metal sensors. Interestingly, CmtA, the protein whose gene is regulated by CmtR<sup>Mtb</sup>, is closely related to *S. aureus* CadA and *E. coli* ZntA, both of which are well characterized Zn<sup>II</sup>/Cd<sup>II</sup>/Pb<sup>II</sup> P<sub>1B</sub>-type ATPase efflux pumps (32, 33).

To gain insight into the mechanism of metalloregulation by CmtR<sup>Mtb</sup>, we have quantitatively characterized the metal- and DNA-binding properties of nearly fully reduced wild-type CmtR<sup>Mtb</sup> and a C102S substitution mutant. Of particular interest was the extent to which CmtR<sup>Mtb</sup> binds Zn<sup>II</sup>, since this metal fails to induce transcription *in vivo* (18). We also present a preliminary characterization of CmtR homolog encoded in the genome of *S. coelicolor* A3(2), termed CmtR<sup>Sc</sup>. The metal binding properties of wild-type CmtR<sup>Sc</sup> and the double mutant C110G/C111S CmtR<sup>Sc</sup>, which converts the two C-terminal residues to nonliganding side chains provides supports for the conclusion that metal binding properties of related sensor proteins can indeed be predicted from amino acid sequence alone. The findings presented in this thesis provide significant new insights into the mechanisms of metal binding, metal selectivity, and metal-mediated negative allosteric regulation of protein-DNA binding in the SmtB/ArsR protein family.

## CHAPTER II

### MATERIALS AND METHODS

#### Materials

*Chemicals.* All buffers were prepared using Milli-Q doubly distilled deionized water. MES, Tris, HEPES and Bis-Tris buffer salts, ammonium sulfate, and 5,5'-dithiobis(2-nitrobenzoic acid) (DTNB<sup>1</sup>) were purchased from Sigma. Chromatography materials were obtained from Pharmacia Biotech. Ultrapure cadmium(II) chloride and lead(II) chloride were acquired from Johnson Matthey. d<sup>18</sup> HEPES and D<sub>2</sub>O were obtained from Cambridge Isotopes.

#### Methods

*Construction of wild-type and C102S CmtR<sup>Mtb</sup> overexpression plasmids.* To create pET3a-CmtR<sup>Mtb</sup>, the CmtR<sup>Mtb</sup> coding region was amplified by PCR from *M. tuberculosis* H37Rv genomic DNA using primers I (5'-GAGTCCATATGCTGACGTGTGAG-3') and II (5'-GTCATGGATCCTCATCAGCTACCTGTC-3') and cloned into pET3a (Novagen) between the *Bam*HI and *Nde*I restriction sites using standard cloning techniques. The C102S CmtR mutant was generated by site-directed mutagenesis method using the QuikChange kit (Stratagene) and primers III (5'-GATACCGACCAACCCTCTGTC-3') and primer IV (5'-GACAGAGGGTTGGTCGGTATC-3') and pET3a-CmtR<sup>Mtb</sup> as template.

*Construction of wild-type and C110G/C111S CmtR<sup>Sc</sup> overexpression plasmids.* To create pET3a-CmtR<sup>Sc</sup>, the CmtR<sup>Sc</sup> coding region was amplified by PCR from

*Streptomyces violaceoruber* genomic DNA (American Type Culture Collection, ATCC) using primers V (5'-AAAAACATATGGTGCTGACTCTCGCTGCCGATATC-3') and VI (5'-AAAAAGCTAAGCTCAGCAGCACTCCTTCTCGTC-3') and cloned into pET3a (Novagen) between the *NdeI* and *BPU1102I* restriction sites using standard cloning techniques. The plasmid encoding C110G/C111S CmtR<sup>Sc</sup> was generated by site-directed mutagenesis method using the QuikChange kit (Stratagene) and primers VII (5'-GGACGAGAAGGAGGGCTCCTGAGCAATAACTAGC-3') and primer VIII (5'-GCTAGTTATTGCTCAGGAGCCCTCCTTCTCGTCC-3') using pET3a-CmtR<sup>Sc</sup> as template.

*Purification of wild type and mutant CmtR<sup>Mtb</sup> and CmtR<sup>Sc</sup>.* pET3a-CmtR<sup>Mtb</sup>-transformed *E. coli* BL21(DE3)/pLysS was grown on a 1.5% LB agar plate containing 0.1 mg/mL ampicillin at 37 °C. A single colony was used for 200 mL overnight seed culture (37 °C) which was subsequently used to inoculate 9 L of LB containing 0.1 mg/mL ampicillin. The cells were grown at 37°C with vigorous aeration to an OD of 0.5-0.6 at 600 nm, after which time 0.4 mM IPTG was added to induce the expression of CmtR<sup>Mtb</sup>. Cells were harvested by low-speed centrifugation and the wet cell paste used for purification. The purification of CmtR<sup>Mtb</sup> was largely adapted from prior procedures for pI258 CadC (22), except 5 mM DTT was used throughout, and the final dialysis carried out in the anaerobic chamber was against 10 mM HEPES, 0.40 M NaCl, pH 7.0. After purification, overloaded SDS-PAGE gels showed a single band at the anticipated molecular weight (12.9 kDa). The concentration of CmtR<sup>Mtb</sup> was determined using the calculated molar extinction coefficient at 280 nm of 5220 M<sup>-1</sup>•cm<sup>-1</sup> (41). Purified

CmtR<sup>Mtb</sup> was stored at -80°C in an anaerobic environment in small aliquots in sealed tubes. C102S CmtR<sup>Mtb</sup>, was purified using the same method except for using *E. coli* Rosetta (DE3) cells were used for protein expression. CmtR<sup>Sc</sup> and C110G/C111S CmtR<sup>Sc</sup> were purified using the same method as CmtR<sup>Mtb</sup>. The theoretical molecular weight for CmtR<sup>Sc</sup> is 12.2 kDa and the extinction coefficient is calculated as 3730 M<sup>-1</sup>•cm<sup>-1</sup> (41).

*Free thiol determination.* A standard DTNB colorimetric assay was used to determine the number of free thiols in CmtR<sup>Mtb</sup> and CmtR<sup>Sc</sup> (42). 25 µL 2.5 mM DTNB solution was added separately into 400 µL 10-15 µM protein. After a 30 min incubation in the anaerobic chamber, the concentration of thiolate anion was quantified at 412 nm ( $\epsilon=13,600 \text{ M}^{-1}\cdot\text{cm}^{-1}$ ) after subtraction of the absorbance of the final dialysis buffer with same concentration of DTNB. The calculated number of free thiols in wild-type and C102S CmtR<sup>Mtb</sup> was found to be  $5.5 \pm 0.2$  (6 expected) and  $4.3 \pm 0.2$  (5 expected) free thiols per monomer. The free thiols in wild-type CmtR<sup>Sc</sup> were  $5.8 \pm 0.2$  (6 expected) and  $3.0 \pm 0.2$  (4 expected) for C110G/C111S CmtR<sup>Sc</sup>.

*Atomic absorption spectroscopy.* The concentrations of all metal titrants were determined using a Perkin-Elmer Analyst 700 atomic absorption spectrophotometer operating in flame mode using a different hollow cathode lamps specific for each metal (42). Zn<sup>II</sup> was detected at 213.9 nm (slit=0.7 nm), Cd<sup>II</sup> was detected at 228.8 nm (slit = 0.7 nm) and Pb<sup>II</sup> was detected at 283.3 nm (slit = 0.7nm).



## CHAPTER III

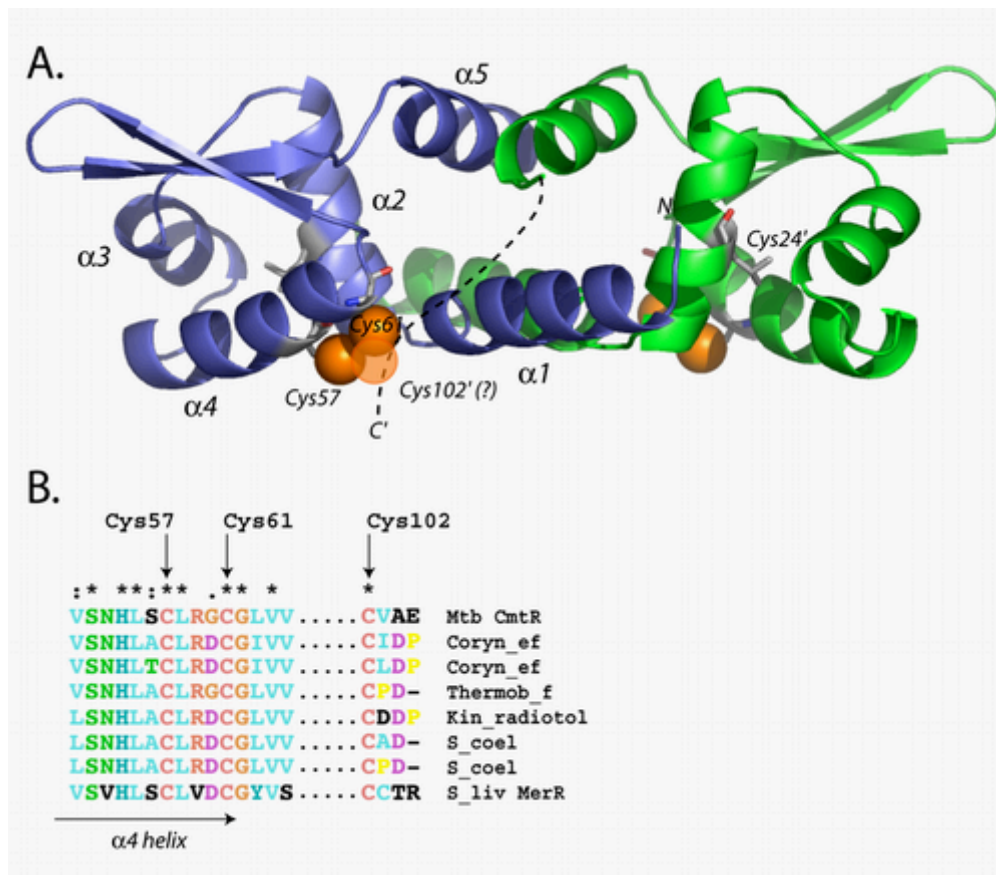
FUNCTIONAL CHARACTERIZATION OF *M. tuberculosis* CmtRVARIANTS: Cys102 IS A KEY METAL LIGAND IN ALLOSTERIC REGULATION  
BUT IN METAL CHELATE STABILIZATION**Introduction**

*Mycobacterium tuberculosis* is a slow growing pathogen that is the causative agent of tuberculosis disease in human(17). There is widespread emergence of drug-resistant strains and has a deadly synergy with human immunodeficiency virus (HIV) (17). The progenitor of *M. tuberculosis* complex, comprised of *M. tuberculosis*, *M. bovis*, *M. bovis* BCG, *M. africanum* and *M. microti*, is thought to have evolved from a soil bacterium that have many common characteristics with the *actinomycetes*, *Streptomyces. coelicolor* (17). *M. tubersulosis* is naturally resistant to many antibiotics and different environments, which is largely a consequence of its nearly impenetrable hydrophobic cell envelope and numerous membrane bound transporters (17).

In 2002, a *M. tuberculosis* Ni<sup>II</sup>/Co<sup>II</sup> sensing repressor in SmtB/ArsR family was reported and designated NmtR (27). CmtR<sup>Mtb</sup> is a Cd<sup>II</sup>/Pb<sup>II</sup> sensor discovered in *M. tuberculosis* in 2003 (18). Before that, the best characterized Cd<sup>II</sup>/Pb<sup>II</sup> metalloregulatory protein was *S. aureus* pI258 CadC. CadC negatively regulates transcription of the *cad* operon which is composed of CadC and CadA encoding genes (32, 43). CadA is a P-type ATPase efflux pump that is specific for Pb<sup>II</sup>, Cd<sup>II</sup> and Zn<sup>II</sup> (32, 43). Analytical sedimentation equilibrium ultracentrifugation reveals pI258 CadC is a stable homodimer in solution (22). Direct Cd<sup>II</sup> binding experiments gave an intense S<sup>-</sup> to Cd(II) ligand-to-

metal charge transfer (LMCT) transitions at 240nm and had a molar absorptivity  $\approx 25000 \text{ M}^{-1} \text{ cm}^{-1}$  (22).  $K_{\text{Cd}}$  was determined to be  $4.3 (\pm 1.8) \times 10^{12} \text{ M}^{-1}$  by virtue of EDTA-protein competition experiments (22).  $^{113}\text{Cd}$  NMR spectroscopy of  $^{113}\text{Cd}^{\text{II}}$ -substituted CadC gives a chemical shift at 622 ppm (22). These data suggests  $\text{Cd}^{\text{II}}$  form a  $\text{S}_4$  coordination complex in CadC but do not eliminate the possibility of an  $\text{S}_3(\text{O})\text{-Cd}^{\text{II}}$  complex (22).  $\text{Pb}^{\text{II}}$  titration to pI258 CadC reveals a long-wavelength absorption band with an absorption maximum at 350 nm ( $\epsilon_{350} \approx 4000 \text{ M}^{-1} \text{ cm}^{-1}$ ), which is most consistent with three or four thiolate ligand- $\text{Pb}^{\text{II}}$  complex (22). Both  $\text{Cd}^{\text{II}}$  and  $\text{Pb}^{\text{II}}$  bind to pI258 CadC in  $\approx 0.7$  metal per monomer stoichiometry (22). These two metal ions are able of allosterically regulating *cad O/P* binding of CadC. Without their presence, a tight dimeric  $(\text{CadC})_2$ -*cad O/P* complex can form with  $K_a = 1.1 (\pm 0.3) \times 10^9 \text{ M}^{-1}$  (22). When protein is saturated with  $\text{Cd}^{\text{II}}$  or  $\text{Pb}^{\text{II}}$ , the binding affinity constant will decreased by  $\approx 300$ -fold (22).

Although structurally distinct from pI258 CadC,  $\text{CmtR}^{\text{Mtb}}$  can also regulate  $\text{Pb}^{\text{II}}/\text{Cd}^{\text{II}}$  concentration in *M. smegmatis* (18). *LacZ* reporter gene assays were performed with several CmtR variants (18). Cys57, Cys61 and Cys102 were shown to be essential for Cd(II)-mediated transcriptional derepression in *M. smegmatis* among total six cysteine residues in  $\text{CmtR}^{\text{Mtb}}$  (18). These cysteines are mapped onto a homology model of  $\text{CmtR}^{\text{Mtb}}$  (Figure 5A); this finding is consistent with the fact only these three Cys are absolutely conserved in putative  $\text{CmtR}^{\text{Mtb}}$  homologs from other bacteria (Figure 5B). Note that Cys61 in the  $\text{CmtR}^{\text{Mtb}}$  homology model (Figure 5A) is just N-terminal to Arg87 of SmtB, a key allosteric residue in the  $\alpha 5$  zinc sensor SmtB (30). A putative



**FIGURE 5:** (A) Homology model of the CmtR<sup>Mtb</sup> homodimer based on the crystal structure of apo-SmtB structure (30, 32). (One CmtR<sup>Mtb</sup> protomer is shaded blue and the other green. The carboxyl-terminus of CmtR<sup>Mtb</sup> can not be modeled and is represented by a dotted line. Important cysteine residues are labeled.) (B) Two windows derived from multiple sequence alignment of CmtR<sup>Mtb</sup> and putative homologs. (Each homolog has three conserved cysteines that correspond to Cys57, Cys61 and Cys102 in the CmtR<sup>Mtb</sup> sequence.)

operator/promoter region that forms a binding site for CmtR<sup>Mtb</sup> was also proposed on the basis of gel mobility shift assay in that study (18).

In this chapter, we focus our attention on understanding the function of Cys102 as a putative metal ligand in CmtR<sup>Mtb</sup>. We used analytical sedimentation equilibrium ultracentrifugation to examine the assemble states of both wild-type and mutant CmtR<sup>Mtb</sup>. We adopted UV-Vis spectroscopy to measure metal binding stoichiometry and affinity constants. We utilized <sup>113</sup>Cd NMR spectroscopy and perturbed angular correlation (PAC) spectroscopy to examine the coordination geometry of Cd<sup>II</sup>-protein complex. Finally, fluorescence anisotropy was used to monitor the allosteric negative regulation event of *cmt O/P* binding by different metal ions. These findings are discussed in the context of previous work on the paradigm Cd<sup>II</sup>/Pb<sup>II</sup> sensor *S. aureus* pI258 CadC.

## Experimental procedures

*Analytical sedimentation equilibrium ultracentrifugation.* A Beckman Optima XL-A analytical ultracentrifuge was used to run all experiments (22), with the rotor speed set to 20,000 rpm at 25.0 °C. Ultracentrifuge cells were assembled in the anaerobic glove box and contained 12 μM apo wild-type CmtR<sup>Mtb</sup> or C102S CmtR<sup>Mtb</sup>. Sedimentation equilibrium data were acquired and evaluated by a nonlinear least-squares fitting program, Microcal Origin. The partial specific volume ( $v$ ) of 0.736 mL/g for CmtR<sup>Mtb</sup>, 0.7361 mL/g for C102S CmtR<sup>Mtb</sup> and a buffer density ( $\rho$ ) of 1.0 g/mL was used in the analysis via global simultaneous fitting to a single ideal species model by Ultrascan. The lower limit of the dimerization equilibrium constant,  $K_{\text{dimer}}$ , was

calculated assuming  $2 P \rightleftharpoons P_2$  and that  $[(1-P)/(1-0.5P)] \cdot M_r^P + [0.5P/(1-0.5P)] \cdot M_r^{P2} = M_r^{\text{observed}}$ , where P is the fractional population of monomer that self-associates into dimer and  $K_{dimer} \text{ (lower limit)} = (0.5 P \cdot C) / [(1- P) \cdot C]^2$ , where C is total protein concentration.

*Cd<sup>II</sup>, Pb<sup>II</sup> optical absorption spectroscopy.* All metal binding experiments were carried out anaerobically at ambient temperature (~25°C) using a Hewlett-Packard model 8452A spectrophotometer (22). For Cd<sup>II</sup> titrations, apoproteins were diluted using final dialysis buffer S to ≈50 μM in 800 μL and loaded into an anaerobic cuvette fitted with a Hamilton gas-tight adjustable volume syringe containing 0.5 mM Cd<sup>II</sup> titrant in the glove box. Complete optical spectra of apo protein were collected from 200-900 nm 1-2 min after each addition of a known aliquot (5-15 μL) of Cd<sup>II</sup>. Corrected spectra were obtained by subtraction of the apoprotein spectra from each spectrum obtained after addition of metal ion, and further corrected for dilution. The binding isotherms were fit to a 1:1 binding model (DynaFit) to obtain lower limit for  $K_{Cd}$ . Pb<sup>II</sup> titrations were done in exactly the same way except that 10 mM bis-tris, 0.4 M NaCl, pH 7.0 was used as the buffer. Bis-Tris is a weak chelating buffer that can prevent excess Pb<sup>II</sup> from forming Pb<sup>II</sup>(OH)<sub>2</sub> precipitate (44). Metal competition experiments performed with either EDTA or EGTA were carried out as described above except that the 200-300 μM chelator was present. The conditional stability constants for various metal-chelator complexes were calculated under these conditions essentially as described (45, 46) with  $K_{Cd}^{EDTA} = 3.2 \times 10^{12} \text{ M}^{-1}$  and  $K_{Pb}^{EGTA} = 1.38 \times 10^{10} \text{ M}^{-1}$ . The resulting optical data were fitted to a simple competition model using DynaFit.

*Zn<sup>II</sup> binding experiments.* The zinc chelator dye magfura-2 ( $K_{Zn} = 5.0 \times 10^7 \text{ M}^{-1}$  at pH 7.0 and 25°C) (25) was used as a colorimetric competitor for Zn<sup>II</sup> binding by wild-type and C102S CmtR<sup>Mtb</sup> essentially as previously described (25). For wild type CmtR<sup>Mtb</sup>, 20  $\mu\text{M}$  CmtR<sup>Mtb</sup> and 18.8  $\mu\text{M}$  magfura-2 were used; for C102S CmtR<sup>Mtb</sup>, 19.8  $\mu\text{M}$  protein and 19  $\mu\text{M}$  magfura-2 were used. The data were fit to a competitive binding model DynaFit to determine the zinc binding affinity  $K_{Zn}$  for both proteins.

*<sup>113</sup>Cd NMR spectroscopy.* The <sup>113</sup>Cd NMR spectrum of CmtR<sup>Mtb</sup> wild type was recorded as previous described (22). The final concentration of <sup>113</sup>Cd(II)-bound CmtR<sup>Mtb</sup> was determined by optical spectroscopy to be 0.8 mM.

*Perturbed angular correlation (PAC) spectroscopy* (carried out collaboratively with Lars Hemmingsen from Department of Natural Science, The Royal Veterinary and Agricultural University, Denmark). PAC spectroscopy was carried out at  $1 \pm 2 \text{ }^\circ\text{C}$ , controlled by a Peltier element. The radioactive <sup>111m</sup>Cd isotope was produced on the day of the experiment at University Hospital cyclotron (Copenhagen), typically 500 MBq at production stop, and extracted as described previously (47). In addition, an HPLC separation (using a TESSEK HEMA 40Q PEEK 7.5 mm  $\times$  75 mm anion exchange column) of the cadmium from other metal ions, most notably zinc ions, was carried out. The <sup>111m</sup>Cd containing fractions were pooled, evaporated to about 50  $\mu\text{L}$ , and mixed with non-radioactive cadmium acetate and MES buffer. The protein was added, and the sample was left to equilibrate for 10 minutes to allow for metal binding, and 55% (w/w) sucrose added in order to slow down rotational tumbling of the molecules. The samples were purged with argon and either used immediately after preparation or left on ice for

up to 3 hours until the measurement was initiated. All buffers were purged with argon and treated so as to lower metal contamination. The final volume of the samples ranged between 0.05 and 0.2 mL with concentrations of 51  $\mu\text{M}$  protein, 10  $\mu\text{M}$   $\text{Cd}^{\text{II}}$ , 53 mM MES, 430 mM NaCl, 55 % (w/w) sucrose, and pH as indicated in table on p38. The pH was measured at room temperature the day after the PAC experiment.

The theoretical and technical aspects of PAC spectroscopy are reviewed in detail in ref. (48) with particular emphasis on biological applications (49). Radioactive  $^{111\text{m}}\text{Cd}$  isotope is used that exploits the angular correlation between the two  $\gamma$ -rays emitted in the nuclear decay. This angular correlation is perturbed by the nuclear quadrupole interaction between the nuclear electric quadrupole moment and the electric field gradient from the surrounding charge distribution. Measuring this perturbed angular correlation provides a fingerprint of the metal ion binding site structure (48, 49). The experimental perturbation function,  $A_2G_2(t)$ , was constructed from coincidence spectra for all combinations of six detectors mounted so that they face the six sides of a cube (47). The background due to accidental coincidences was subtracted in each spectrum and time calibration was carried out using a  $^{75}\text{Se}$  source. The theoretical expression for the perturbation function for randomly oriented molecules contains five parameters which were fitted to the experimental perturbation function using a conventional  $\chi^2$  method (47). The parameters fitted to the experimental data are:  $\omega_0$ , a measure of the nuclear quadrupole interaction strength;  $\eta$ , the so-called asymmetry parameter (always between 0 and 1 in magnitude, and 0 for axially symmetric complexes);  $\Delta\omega_0/\omega_0$ , the frequency spread, assuming a Gaussian distribution around  $\omega_0$

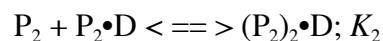
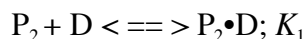
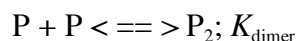
with width  $\Delta\omega_0/\omega_0$ , describing small structural variations from molecule to another;  $\tau_c$ , the rotational correlation time of the molecule; and A, the amplitude of the signal. The fits were carried out using 400 data points, excepting the first 5 points due to systematic errors. For the C102S CmtR<sup>Mtb</sup> mutant the rotational correlation time was constrained to be the same for the two NQIs recovered from the fits.

*Fluorescence anisotropy.* All fluorescence anisotropy experiments were carried out with an ISS PC1 Photon Counting Spectrofluorometer operating in the L-format. A 40-mer, double-stranded *cmt* O/P oligonucleotide (5) (Qiagen) used was 5'-end labeled with fluorescein as indicated on the sequence below:

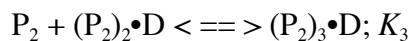
5' - [ F ] - CAAATAGTACACCATATACTGGTATAACAGCAAGAGCTGA - 3'

3' - GTTTATCATGTGGTATATGACCATATTGTCGTTCTCGACT - 5'

The 10-5-10 inverted repeat previously proposed to be critical for the binding of CmtR<sup>Mtb</sup> is underlined (18). Apo-CmtR<sup>Mtb</sup> or Cd<sup>II</sup>-CmtR<sup>Mtb</sup> (preformed stoichiometric complexes) were used as titrants into 1.8 mL of 20 nM or 80 nM *cmt* O/P at 25.0 °C. For the apoprotein titrations, the binding buffer contained 10 mM HEPES, 0.4 M NaCl, 1.0 mM DTT, 50  $\mu$ M EDTA, pH 7.0. For the Cd<sup>II</sup>-protein titrations, EDTA was absent from the buffer and replaced by 10  $\mu$ M Cd<sup>II</sup>. Anisotropy data were fit using the program DynaFit to a dissociable dimer (P<sub>2</sub>) model with a limiting 3:1 P<sub>2</sub>•D binding stoichiometry linked to the monomer-dimer equilibrium (20):



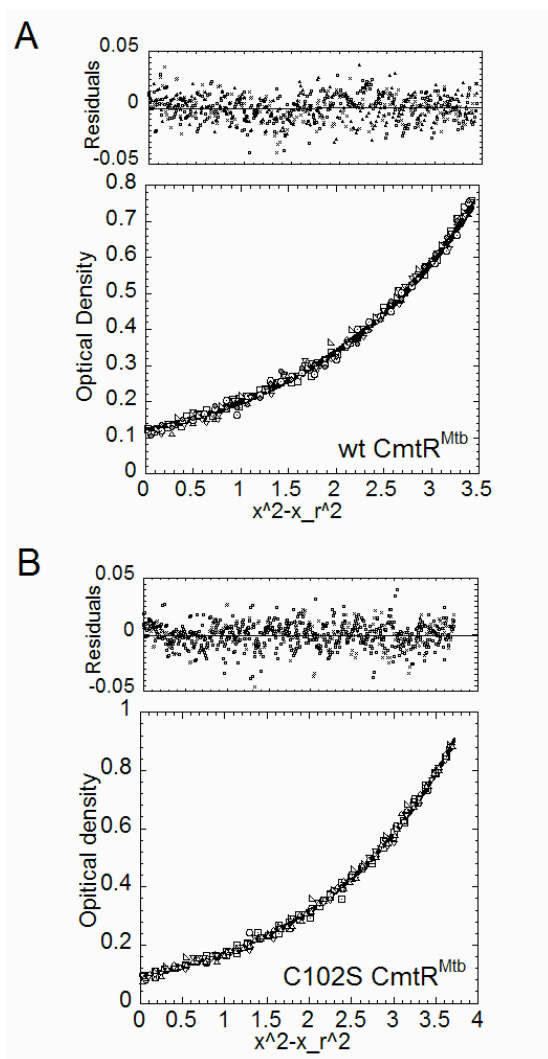




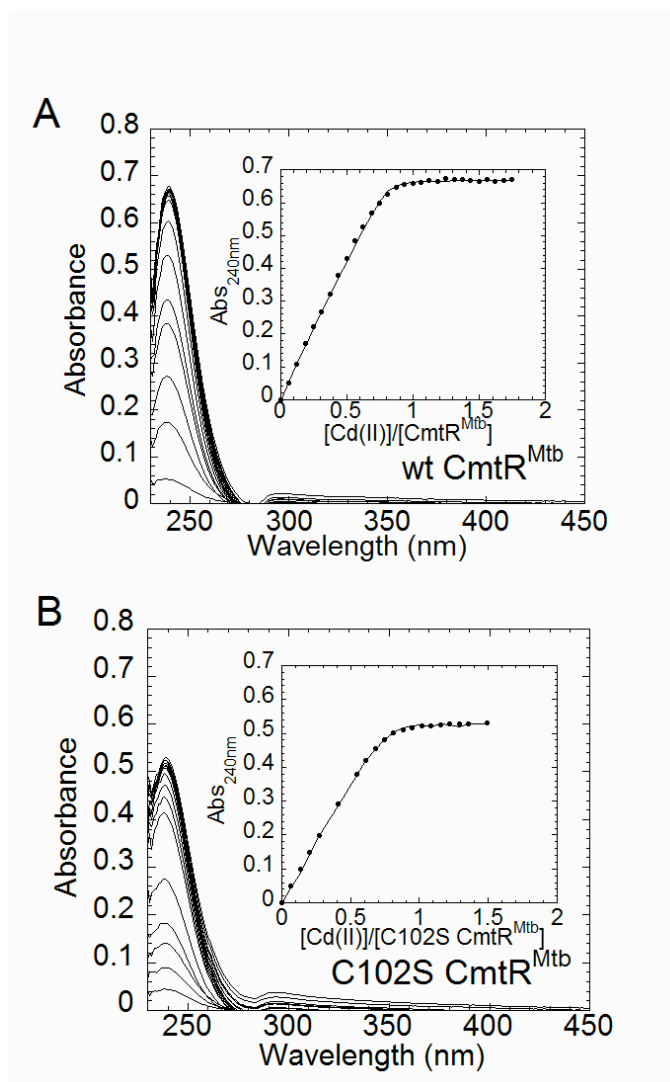
In these fits,  $K_{\text{dimer}}$  was fixed to the lower limits determined by analytical sedimentation equilibrium ultracentrifugation where  $K_{\text{dimer}} = 1.7 \times 10^7 \text{ M}^{-1}$  both wild-type CmtR<sup>Mtb</sup> and C102S CmtR<sup>Mtb</sup>. The characteristic anisotropy,  $r_i$ , for each  $(P_2)_n \bullet D$  complex was estimated by stoichiometric additions of wild-type CmtR<sup>Mtb</sup> and C102S CmtR<sup>Mtb</sup> to a high concentration of *cmt* O/P fragment (10  $\mu\text{M}$ ). The results of these titrations gave  $r_{P_2 \bullet D} = 0.092$ ,  $r_{(P_2)_2 \bullet D} = 0.110$ ,  $r_{(P_2)_3 \bullet D} = 0.135$  for wild-type and  $r_{P_2 \bullet D} = 0.104$ ,  $r_{(P_2)_2 \bullet D} = 0.120$ ,  $r_{(P_2)_3 \bullet D} = 0.148$  for C102S CmtR<sup>Mtb</sup>, with the  $r_D = 0.082$  for free DNA. Each  $r_i$  was treated as fixed parameters to obtain  $K_i$  for each binding step. If  $r_D$  was not exactly equal to 0.082 in any particular experiment, all  $r_i$  values were adjusted up or down accordingly by  $\leq 0.003$  (26).

## Results

*Assembly state of wild-type and C102S CmtR<sup>Mtb</sup>.* Both CmtR<sup>Mtb</sup> variants were subjected to analytical equilibrium sedimentation ultracentrifugation at 20,000 rpm at 12  $\mu\text{M}$  monomer concentration under conditions of pH and temperature (pH 7.0, 25.0 °C) identical to the metal binding and DNA binding experiments. Absorbance was recorded at 237 nm with the results shown in Figure 6. Each set of experimental data that had reached equilibrium was then subjected to a global simultaneous fit to a single ideal species model which is shown by a solid line. The apparent molecular weights obtained 24,750 (expected 25,956.1 g/mol) and 26,540 g/mol (expected 25,923.9 g/mol), for wild-type and C102S CmtR<sup>Mtb</sup>, respectively. These data reveal that both apo-CmtR<sup>Mtb</sup>



**FIGURE 6:** Analytical sedimentation equilibrium ultracentrifugation of (A) apo-wild type CmtR<sup>Mtb</sup> and (B) apo-C102S CmtR<sup>Mtb</sup>. The protein concentration in each case was 12  $\mu$ M monomer. Filled symbols represent an overlay of the data collected during the last five scans, indicative that equilibrium had been reached. The solid line represents the global simultaneous fit for a single ideal species model using Ultrascan. For wild-type CmtR, the fitted molecular weight ( $M_w$ ) is 24750 D (theoretical dimer  $M_w = 25956$  D), variance =  $1.5590 \times 10^{-4}$ . For apo-C102S CmtR, the fitted  $M_w = 26540$  D (theoretical dimer  $M_w = 25924$  D), variance =  $1.1885 \times 10^{-4}$ . Conditions: 10 mM HEPES, 0.4 M NaCl, 0.1 mM EDTA pH 7.0, 25°C at 20,000 rpm rotor speed.

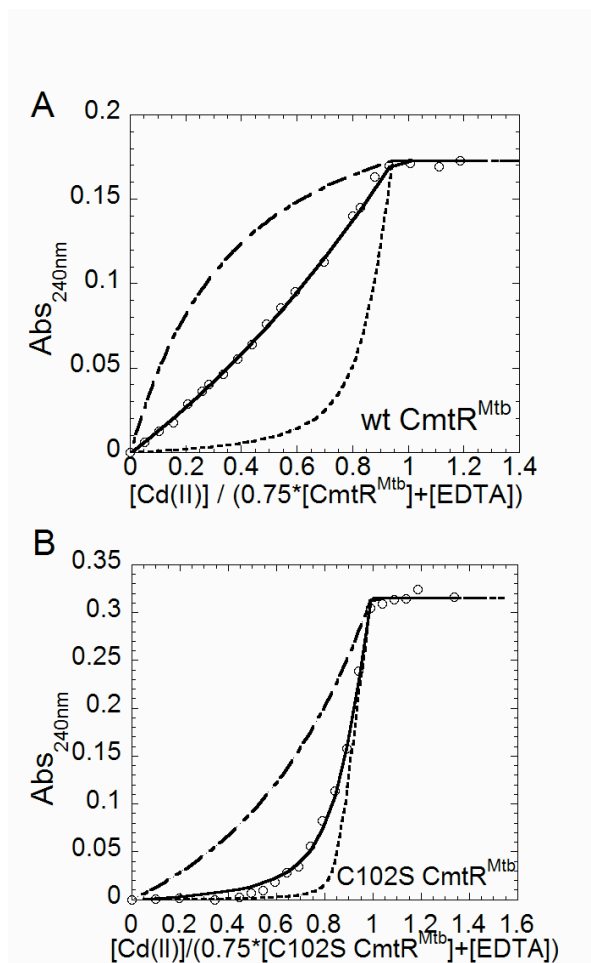


**FIGURE 7:** Representative anaerobic Cd<sup>II</sup> titrations of (A) apo wild-type CmtR<sup>Mtb</sup> (49.4  $\mu$ M) and (B) apo C102S CmtR<sup>Mtb</sup> (47.3  $\mu$ M). (A) Full corrected ultraviolet absorption spectra that result from increasing additions of Cd<sup>II</sup> are shown. (Inset) Cd<sup>II</sup> binding isotherm plotted a change in  $A_{240}$  versus. [CmtR<sup>Mtb</sup> monomer]. For wild-type CmtR<sup>Mtb</sup> (panel A), the solid curve represents the fit to a 1:1 binding model that returns the following parameters:  $K_{\text{Cd-CmtR}_{\text{Mtb}}} = 9.9 (\pm 2.3) \times 10^6 \text{ M}^{-1}$  (a lower limit under these conditions) and active [CmtR<sup>Mtb</sup> monomer] = 37.2 ( $\pm 0.1$ )  $\mu$ M. For C102S CmtR<sup>Mtb</sup> (panel B), the solid curve defines a fit to a 1:1 binding model with  $K_{\text{Cd-C102SCmtR}_{\text{Mtb}}} = 3.2 (\pm 0.4) \times 10^6 \text{ M}^{-1}$  (a lower limit) and active [C102S CmtR<sup>Mtb</sup> monomer] = 33.4 ( $\pm 0.2$ )  $\mu$ M. Conditions: 10 mM HEPES, 0.4 M NaCl, at pH 7.0, 25°C.

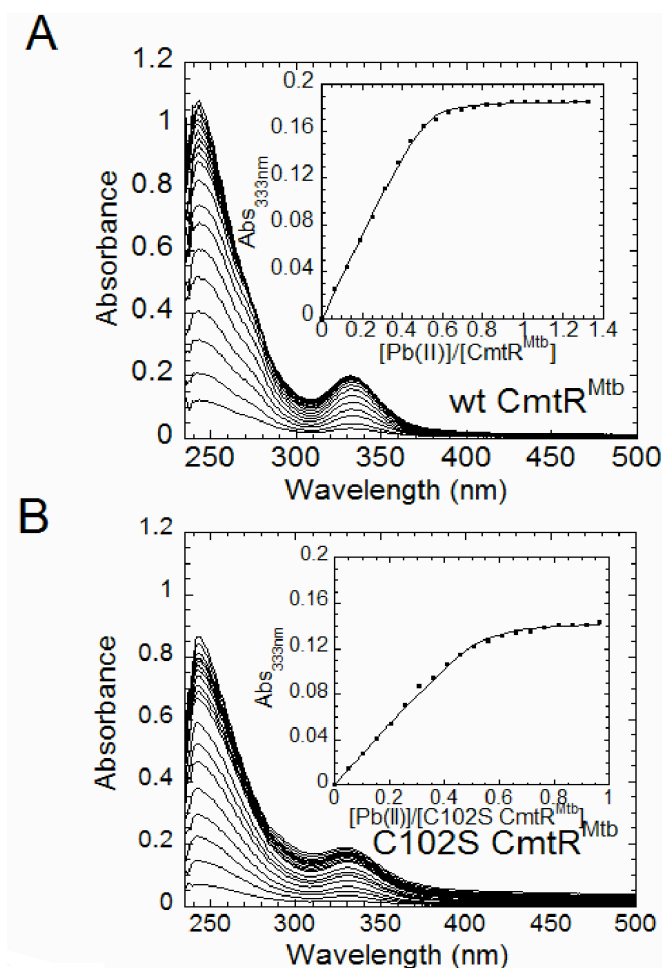
and apo-C102S CmtR<sup>Mtb</sup> exist primarily as stable homodimers under these conditions. Because the monomer concentration is too low under these conditions to accurately measure, only a lower limit of  $K_{\text{dimer}}$  of  $1.7 \times 10^7 \text{ M}^{-1}$  could be obtained from these data.

*Cd<sup>II</sup> optical spectroscopy.* Shown in Figure 7 are representative absorption spectra that result from anaerobic Cd<sup>II</sup> binding titration of  $\approx 50 \mu\text{M}$  apo-wild-type CmtR<sup>Mtb</sup> (Figure 7A) and C102S CmtR<sup>Mtb</sup> (Figure 7B). Binding isotherms (*insets*) were obtained by plotting the corrected absorbance at 240 nm as a function of [Cd<sup>II</sup>]/[CmtR<sup>Mtb</sup>] or [Cd<sup>II</sup>]/[C102S CmtR<sup>Mtb</sup>] ratio. As can be seen, both spectral titrations with Cd<sup>II</sup> result in intense absorption in the ultraviolet, assignable to S<sup>-</sup> to Cd<sup>II</sup> ligand-to-metal charge transfer (LMCT<sup>1</sup>) transition. Cd<sup>II</sup> binds with an apparent stoichiometry of  $\approx 0.75 \text{ Cd}^{\text{II}}:\text{CmtR}^{\text{Mtb}}$  monomer in both cases. The simplest interpretation of a nonintegral stoichiometry is partial inactivation of metal sites due to some cysteine oxidation (see Materials and Methods), as previously observed for CadC (22). We see no evidence for the presence of a second cysteine-containing Cd<sup>II</sup> site in CmtR<sup>Mtb</sup> as found previously (18). Molar absorptivities are  $\approx 16,000 \text{ M}^{-1}\cdot\text{cm}^{-1}$  for wild-type CmtR<sup>Mtb</sup>, and  $\approx 12,000 \text{ M}^{-1}\cdot\text{cm}^{-1}$  for C102S CmtR<sup>Mtb</sup>, both of which are less intense than the tetrathiolate Cd<sup>II</sup> coordination complex in pI258 CadC (22). Using a value of  $\approx 5500 \text{ M}^{-1}\cdot\text{cm}^{-1}$  for each Cd-S coordination bond (50, 51), these data are most consistent with three thiolate ligands in wild-type CmtR<sup>Mtb</sup>, and just two in C102S CmtR<sup>Mtb</sup>.

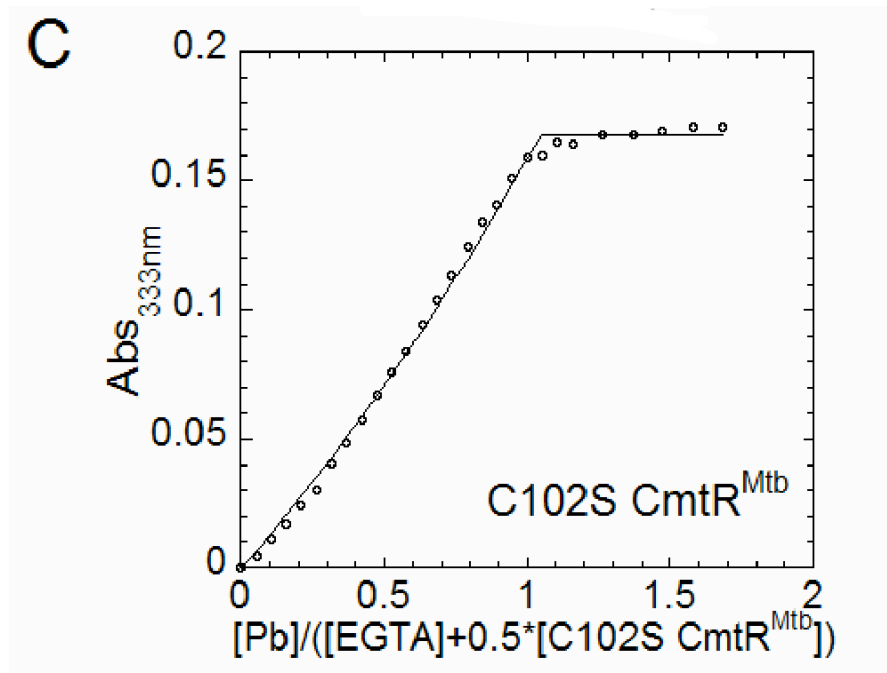
Nonlinear least squares fit of the binding isotherms shown in Figure 7 to a simple 1:1 metal binding model. This simple model was used because the Cd<sup>II</sup> binding is essentially stoichiometric under these conditions and the determined stoichiometry is



**FIGURE 8:** Representative  $\text{Cd}^{\text{II}}$  competition assays carried out with wild-type  $\text{CmtR}^{\text{Mtb}}$  ( $19.9 \mu\text{M}$ ) (A) and C102S  $\text{CmtR}^{\text{Mtb}}$  ( $34 \mu\text{M}$ ) (B) in presence of  $227 \mu\text{M}$  EDTA. The Cd-EDTA complex is transparent in this assay. The solid line represents a nonlinear least-squares fit to a model that assumes one class of  $\text{Cd}^{\text{II}}$  binding sites on the  $\text{CmtR}^{\text{Mtb}}$  homodimer that takes into account the fractional population of active metal binding sites (*i.e.*, 0.75 per monomer; see Fig. 3) and a conditional Cd-EDTA stability constant,  $K_{\text{Cd-EDTA}}$ , of  $3.2 \times 10^{12} \text{ M}^{-1}$ .  $K_{\text{Cd-CmtR}^{\text{Mtb}}} = 1.66 (\pm 0.04) \times 10^{12} \text{ M}^{-1}$ ,  $K_{\text{Cd-C102S CmtR}^{\text{Mtb}}} = 1.03 (\pm 0.09) \times 10^{11} \text{ M}^{-1}$ . Broken lines in each panel represent simulated curves characterized by a  $K_{\text{Cd-protein}}$  of (A)  $1 \times 10^{13} \text{ M}^{-1}$  (— —) and  $1 \times 10^{11} \text{ M}^{-1}$  (- - -), (B)  $1 \times 10^{12} \text{ M}^{-1}$  (— —) and  $1 \times 10^{10} \text{ M}^{-1}$  (- - -)



**FIGURE 9:** Representative anaerobic  $\text{Pb}^{\text{II}}$  titrations of (A) apo wild-type  $\text{CmtR}^{\text{Mtb}}$  ( $48.5 \mu\text{M}$ ), (B) apo C102S  $\text{CmtR}^{\text{Mtb}}$  ( $56.8 \mu\text{M}$ ) and (C) apo C102S  $\text{CmtR}^{\text{Mtb}}$  ( $55.1 \mu\text{M}$ ) and  $91.2 \mu\text{M}$  EGTA. (A) Full corrected ultraviolet absorbance spectra obtained following increasing amounts of added  $\text{Pb}^{\text{II}}$  are shown. *Inset*,  $\text{Pb}^{\text{II}}$  binding isotherm plotted a change in  $A_{333}$  vs. [ $\text{CmtR}^{\text{Mtb}}$  monomer]. For wild-type  $\text{CmtR}^{\text{Mtb}}$  (*panel A*), the solid curve represents the fit to a 1:1 binding model that returns the following parameters:  $K_{\text{Pb-CmtR}^{\text{Mtb}}} = 4.6 (\pm 0.6) \times 10^6 \text{ M}^{-1}$  (a lower limit) and active [ $\text{CmtR}^{\text{Mtb}}$  monomer] =  $23.3 (\pm 0.1) \mu\text{M}$ . For C102S  $\text{CmtR}^{\text{Mtb}}$  (*panel B*), the solid curve defines a fit to a 1:1 binding model with  $K_{\text{Pb-C102S CmtR}^{\text{Mtb}}} = 2.2 (\pm 0.4) \times 10^6 \text{ M}^{-1}$  and active [C102S  $\text{CmtR}^{\text{Mtb}}$  monomer] =  $28.7 (\pm 0.3) \mu\text{M}$ . Wild-type  $\text{CmtR}^{\text{Mtb}}$  binds stronger to  $\text{Pb}^{\text{II}}$  than does EGTA (data not shown) but C102S  $\text{CmtR}^{\text{Mtb}}$  shows a binding affinity of  $\text{Pb}^{\text{II}}$  that is comparable to EGTA (*panel C*). The solid line represents a nonlinear least-squares fit to a model that assumes one major  $\text{Pb}^{\text{II}}$  binding sites per nondissociable  $\text{CmtR}^{\text{Mtb}}$  dimer (*i.e.*, 0.5 per monomer; see panel A) and a conditional  $\text{Pb}$ -EGTA stability constant,  $K_{\text{Pb-EGTA}} = 1.38 \times 10^{10} \text{ M}^{-1}$  (see Material and Methods).  $K_{\text{Pb-C102S CmtR}^{\text{Mtb}}} = 8.7 (\pm 0.4) \times 10^9 \text{ M}^{-1}$ . Conditions: 10 mM Bis-tris, 0.4 M NaCl, pH 7.0,  $25^\circ\text{C}$ .



**FIGURE 9** continued.

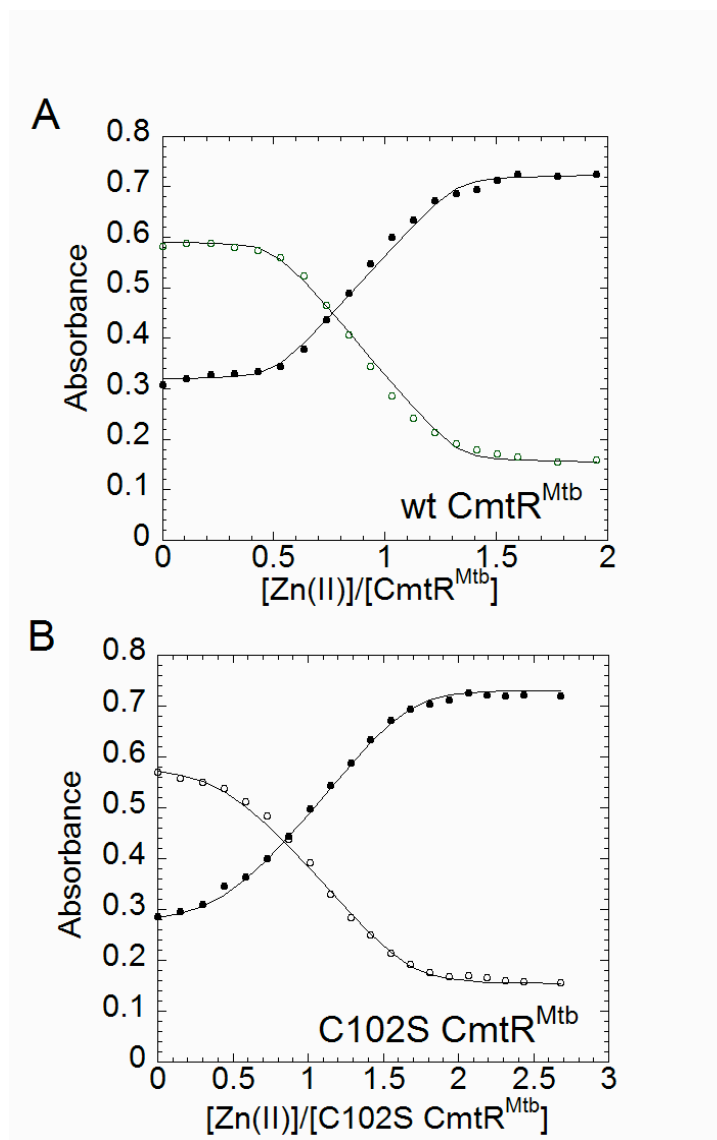
less than unity; however, only a lower limit for  $K_{Cd}$  can be obtained. The same experiment was therefore repeated in the presence of a large molar excess of EDTA (Figure 8), with the conditional  $Cd^{II}$ -EDTA stability constant of  $K_{Cd-EDTA} = 3.2 \times 10^{12} M^{-1}$  under these solution conditions. Formation of the  $Cd^{II}$ -EDTA complex is transparent under these conditions. Nonlinear least squares fitting to a simple competition model (see Materials and Methods) reveals that  $K_{Cd}$  for wild-type CmtR<sup>Mtb</sup> is  $1.71 (\pm 0.05) \times 10^{12} M^{-1}$  (Figure 8A); while  $K_{Cd}$  for C102S CmtR<sup>Mtb</sup> is  $9.9 (\pm 0.8) \times 10^{10} M^{-1}$  (Figure 8B), or  $\approx$  20-fold weaker. These data collectively suggest that Cys102 forms a coordination bond to the  $Cd^{II}$  ion in CmtR<sup>Mtb</sup>, but substitution with a nonliganding side chain reduces the stability of the  $Cd^{II}$  complex by just 10% in free energy (16.7 vs. 15.0 kcal•mol<sup>-1</sup> for wild-type and C102S CmtR<sup>Mtb</sup>, respectively). Interestingly,  $K_{Cd}$  for CmtR<sup>Mtb</sup> is comparable to that previously determined for *S. aureus* pI258 CadC under the same solution conditions (22).

*Pb<sup>II</sup> optical spectroscopy.* Figure 9 shows representative absorption spectra that are obtained upon anaerobic titration of  $Pb^{II}$  to  $\approx 50 \mu M$  apo-wild-type CmtR<sup>Mtb</sup> (Figure 9A) and C102S CmtR<sup>Mtb</sup> (Figure 9B). As above, binding isotherms (*insets*) were obtained by plotting the corrected absorbance at 333 nm as a function of  $[Pb^{II}]/[CmtR^{Mtb}]$  or  $[Pb^{II}]/[C102S CmtR^{Mtb}]$  ratio. The saturated  $Pb^{II}$  absorption spectra for both proteins are characterized by two distinct features: an intense absorption in the far-ultraviolet and a long-wavelength absorption band with maximum at 333 nm ( $\epsilon_{333} = 7900 M^{-1} cm^{-1}$ ), with an overall molar absorptivity again less in the C102S mutant ( $\epsilon_{333} = 4900 M^{-1} cm^{-1}$ ). These intense ultraviolet transitions are thought to result from a combination of  $S^{-}$  to  $Pb^{II}$



ligand-to-metal and metal-to-ligand charge transfer transitions and  $\text{Pb}^{\text{II}}$  intraatomic transitions, *e.g.*,  $\text{Pb}^{\text{II}}$  6s orbital to  $\text{Pb}^{\text{II}}$  6p orbital (52). Unlike the case for  $\text{Cd}^{\text{II}}$ , the extent to which the absorption maximum and intensity reports on coordination number and geometry for  $\text{Pb}^{\text{II}}$ -thiolate complexes is not yet firmly established. However, compared to the structurally characterized  $\text{Pb}^{\text{II}}\text{-S}_3$  trigonal complex of pI258 CadC, the long-wavelength absorption band of  $\text{CmtR}^{\text{Mtb}}$  is blue-shifted relative to wild-type CadC and is quite similar to the  $\text{S}_2(\text{O/N})$  complex formed by C60G CadC (29). In any case, since the molar absorptivity is reduced in C102S  $\text{CmtR}^{\text{Mtb}}$ , these data argue that Cys102 likely donates a ligand to the  $\text{Pb}^{\text{II}}$  ion as well.

The binding titrations for wild-type  $\text{CmtR}^{\text{Mtb}}$  (Figure 9A, *inset*) and C102S  $\text{CmtR}^{\text{Mtb}}$  (Figure 9B, *inset*) reveals the apparent stoichiometry of  $\text{Pb}^{\text{II}}$  binding in both cases is  $\approx 0.5$ , or  $\approx 1$  per homodimer, with a  $K_{\text{pb}} \geq 10^6 \text{ M}^{-1}$  for both proteins. Chelator competition experiments like that shown in Figure 8 with  $\text{Pb}^{\text{II}}$ -EDTA ( $K_{\text{pb-EDTA}}=2.9 \times 10^{14} \text{ M}^{-1}$ ) and  $\text{Pb}^{\text{II}}$ -EGTA<sup>1</sup> ( $K_{\text{pb-EGTA}}=1.38 \times 10^{10} \text{ M}^{-1}$ ) mixtures effectively bracket  $K_{\text{pb}}$  for wild-type  $\text{CmtR}^{\text{Mtb}}$  in the  $10^{13} \sim 10^{12} \text{ M}^{-1}$  range (data not shown). For C102S  $\text{CmtR}^{\text{Mtb}}$ , an EGTA-C102S  $\text{CmtR}^{\text{Mtb}}$  competition experiment reveals a  $K_{\text{pb}}$  comparable to that of EGTA, or  $K_{\text{pb}}=8.7 (\pm 0.4) \times 10^9 \text{ M}^{-1}$ , or  $\approx 100$ -1000-fold weaker than wild-type  $\text{CmtR}^{\text{Mtb}}$  (Figure 9C). The origin of the 0.5:1  $\text{Pb}^{\text{II}}:\text{CmtR}^{\text{Mtb}}$  monomer stoichiometry is unknown, but is unlikely to be due to competition between  $\text{CmtR}^{\text{Mtb}}$  and bis-tris buffer, a weakly chelating buffer used to prevent  $\text{Pb}(\text{OH})_2$  precipitation during the experiment, since varying the buffer concentration (from 5-20 mM) has no effect on the stoichiometry (data not shown). The simplest interpretation is that there is just one high affinity  $\text{Pb}^{\text{II}}$

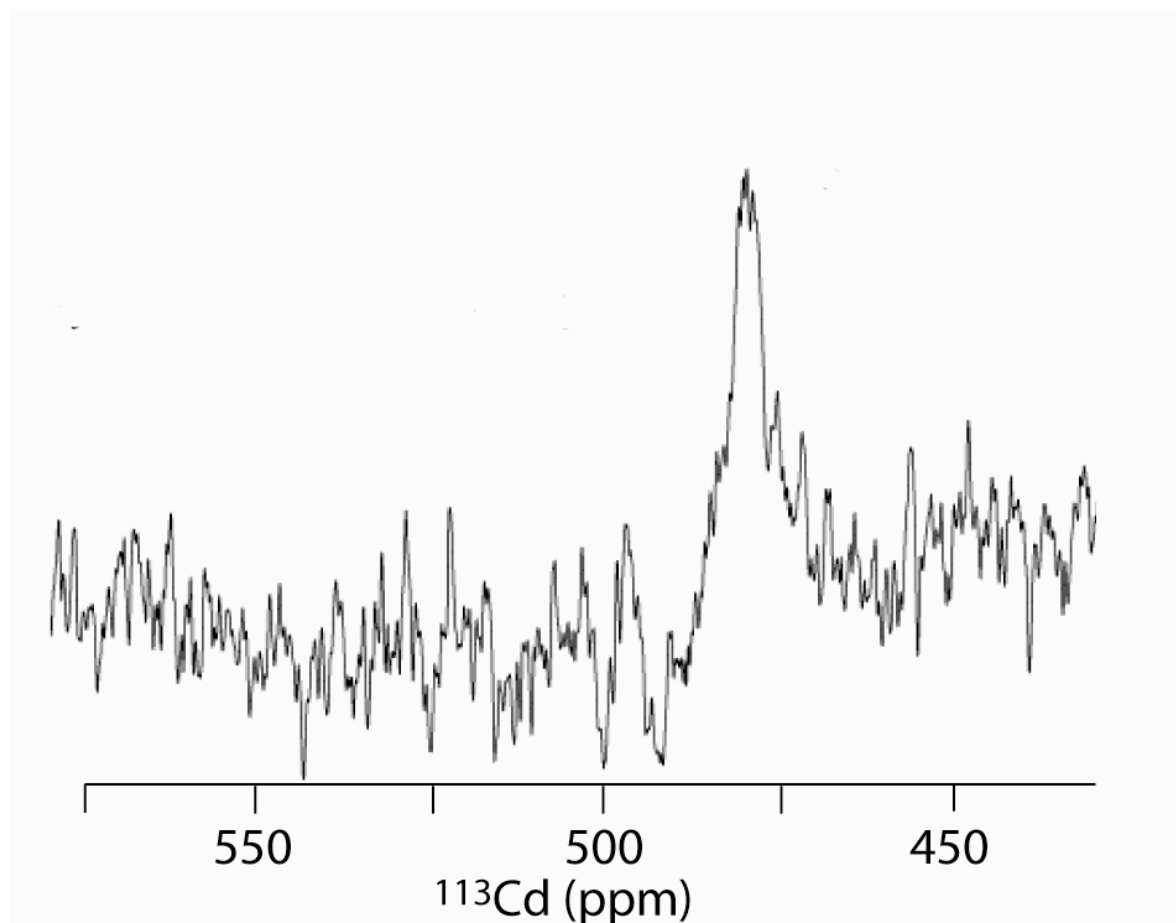


**FIGURE 10:** Representative titrations of  $\text{Zn}^{\text{II}}$  into a mixture of mag-fura-2 and either (A) wild-type  $\text{CmtR}^{\text{Mtb}}$  or (B) C102S  $\text{CmtR}^{\text{Mtb}}$ . In (A),  $22.8 \mu\text{M}$   $\text{CmtR}^{\text{Mtb}}$  and  $18.8 \mu\text{M}$  mag-fura-2 and (B)  $17.8 \mu\text{M}$  C102S  $\text{CmtR}^{\text{Mtb}}$  and  $19.0 \mu\text{M}$  magfura-2 were present. In both panels, the filled circles represent  $A_{325}$  and the empty circles represent  $A_{366}$ . The solid line represents a global non-linear least square fit to a model that incorporates the stepwise binding of two  $\text{Zn}^{\text{II}}$  (defined by  $K_{\text{Zn.P2}}$  and  $K_{\text{Zn2P2}}$ ) to a nondissociable  $\text{CmtR}^{\text{Mtb}}$  dimer using Dynafit. For wild-type  $\text{CmtR}^{\text{Mtb}}$ , the following parameters were obtained:  $K_{\text{Zn.P2}} = 8.5 (\pm 4.1) \times 10^9 \text{ M}^{-1}$  (a lower limit under these conditions),  $K_{\text{Zn2P2}} = 3.0 (\pm 1.5) \times 10^5 \text{ M}^{-1}$ . For C102S  $\text{CmtR}^{\text{Mtb}}$ ,  $K_{\text{Zn.P2}} = 6.5 (\pm 1.3) \times 10^8 \text{ M}^{-1}$ ,  $K_{\text{Zn2P2}} = 8.0 (\pm 3.8) \times 10^5 \text{ M}^{-1}$ . Conditions: 10 mM HEPES and 0.4 M NaCl at pH 7.0 and  $25^\circ\text{C}$ .

site on the homodimer, or more formally, strong negative cooperativity of  $\text{Pb}^{\text{II}}$  binding where the affinity of the second  $\text{Pb}^{\text{II}}$  ion is  $\leq 10^3 \text{ M}^{-1}$ . Negative cooperativity of metal ion binding have previously been previously observed for other homodimeric SmtB/ArsR metal sensors (22, 30).

*Zn<sup>II</sup> binding affinities obtained via chelator competition experiments with magfura-2.* Since previous functional experiments showed that  $\text{Zn}^{\text{II}}$  was not a strong inducer of  $\text{CmtR}^{\text{Mtb}}$ -regulated reporter gene transcription *in vivo*, it was of interest to determine if  $\text{CmtR}^{\text{Mtb}}$  binds  $\text{Zn}^{\text{II}}$  with high affinity. In these experiments, the well-characterized zinc indicator dye magfura-2 ( $K_{\text{Zn} \cdot \text{mag-fura-2}} = 5.0 \times 10^7 \text{ M}^{-1}$ ) was used as a competitor of  $\text{Zn}^{\text{II}}$  binding to  $\text{CmtR}^{\text{Mtb}}$  and C102S  $\text{CmtR}^{\text{Mtb}}$  so that the  $\text{Zn}^{\text{II}}$  binding stoichiometry and affinity constant  $K_{\text{Zn}}$  could be determined (25).

Figure 10 shows representative titrations of  $\text{Zn}^{\text{II}}$  into approximately equimolar mixtures of wild-type  $\text{CmtR}^{\text{Mtb}}$  (Figure 10A) and C102S  $\text{CmtR}^{\text{Mtb}}$  (Figure 10B) and magfura-2. The solid curves represent a fit to a model that describes the binding of two successive  $\text{Zn}^{\text{II}}$  ions to a dissociable  $\text{CmtR}^{\text{Mtb}}$  dimer, the affinities of which are defined by  $K_{\text{ZnP}_2}$  and  $K_{\text{Zn}_2\text{P}_2}$  (see Materials and Methods). Estimated parameters from these experiments are  $K_{\text{ZnP}_2} = 8.5 (\pm 4.1) \times 10^9 \text{ M}^{-1}$ ,  $K_{\text{Zn}_2\text{P}_2} = 3.0 (\pm 1.5) \times 10^5 \text{ M}^{-1}$  for wild-type  $\text{CmtR}^{\text{Mtb}}$  and  $K_{\text{Zn.P}_2} = 6.5 (\pm 1.3) \times 10^8 \text{ M}^{-1}$ ,  $K_{\text{Zn}_2\text{P}_2} = 8.0 (\pm 3.8) \times 10^5 \text{ M}^{-1}$  for C102S  $\text{CmtR}^{\text{Mtb}}$ .  $K_{\text{Zn}_1}$  of  $\approx 1 \times 10^{10} \text{ M}^{-1}$  determined from this approach with magfura-2 provides a reasonable estimate for wild-type  $\text{CmtR}^{\text{Mtb}}$ , since  $K_{\text{Zn}_1}$  was found to be  $\approx 10^{10} \text{ M}^{-1}$  from parallel quin-2<sup>1</sup> titrations (data not shown). As can be seen, both  $\text{CmtR}^{\text{Mtb}}$  homodimers bind  $\text{Zn}^{\text{II}}$  with negative cooperativity, with an effective stoichiometry of tight binding



**FIGURE 11:**  $^{113}\text{Cd}$  NMR spectrum of  $^{113}\text{Cd}$ -substituted  $\text{CmtR}^{\text{Mtb}}$ . Conditions: 0.8 mM  $^{113}\text{Cd}$ -substituted  $\text{CmtR}^{\text{Mtb}}$  in 5 mM  $\text{d}^{18}\text{HEPES}$ , 0.35 M  $\text{NaCl}$ , 10%  $\text{D}_2\text{O}$ , pH 7.0, 25.0 °C. The chemical shift is reported relative to 0.10 M  $\text{Cd}(\text{ClO}_4)_2$ , pH 7.0.

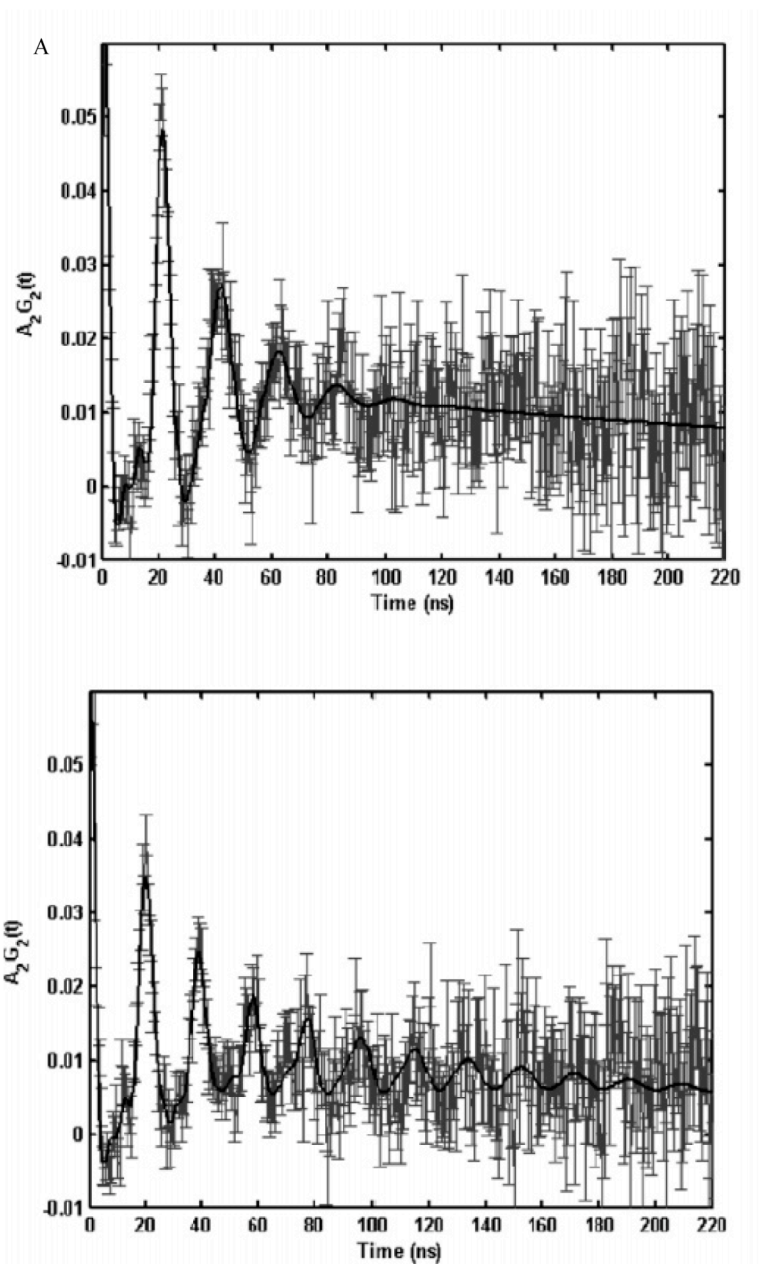
sites of  $\approx 0.5:1$  or  $\approx 1$  per homodimer, with the second  $\text{Zn}^{\text{II}}$  binding site characterized by an affinity less than mag-fura-2. Just like the case for strongly inducing metals  $\text{Cd}^{\text{II}}$ , the affinity of C102S CmtR<sup>Mtb</sup> for  $\text{Zn}^{\text{II}}$  is only  $\approx 10$ -fold lower than wild-type CmtR<sup>Mtb</sup>, but still quite tight. However, for comparison,  $K_{\text{Zn}\cdot\text{P2}}$  determined for two previously characterized  $\text{Zn}^{\text{II}}$  sensors, CzrA and SmtB, is on the order of  $10^{12}$ - $10^{14}$   $\text{M}^{-1}$  (25, 30); thus, CmtR<sup>Mtb</sup> binds  $\text{Zn}^{\text{II}}$  with an affinity that is clearly weaker than other *bona fide* zinc sensors (see Discussion).

*<sup>113</sup>Cd NMR spectroscopy of <sup>113</sup>Cd(II) bound CmtR<sup>Mtb</sup>.* <sup>113</sup>Cd NMR spectroscopy of <sup>113</sup>Cd-substituted metalloproteins provides direct insight into the nature and number of coordinating atoms by virtue of magnitude of <sup>113</sup>Cd chemical shift ( $\delta$ ) (53). In particular, thiolate ligands are more deshielding relative to other ligands, *e.g.*, oxygen and nitrogen, and therefore induce a strongly downfield shifted chemical shift relative to aqueous  $\text{Cd}(\text{ClO}_4)_2$  (53). <sup>113</sup>Cd-substituted wild-type CmtR<sup>Mtb</sup> shows a single broad resonance at  $\delta=480$  ppm (Figure 11). This is 132 ppm upfield of <sup>113</sup>Cd-substituted *L. monocytogenes* CadC (data not shown) and *S. aureus* pI258 CadC (22), each of which are characterized by three strong thiolate donor atoms. The  $\delta$  for <sup>113</sup>Cd-substituted CmtR<sup>Mtb</sup> is therefore more consistent with two strong thiolate donor atoms, likely derived from Cys57 and Cys61 (see Discussion). Repeated attempts to observe a <sup>113</sup>Cd resonance for C102S CmtR<sup>Mtb</sup> were unsuccessful under a variety of solution conditions, presumably due to chemical exchange broadening (data not shown).

*Perturbed angular correlation (PAC) spectroscopy of <sup>111m</sup>Cd-substituted CmtR<sup>Mtb</sup> and C102S CmtR<sup>Mtb</sup>.* The fitted experimental PAC spectra for wild-type and

C102S CmtR<sup>Mtb</sup> are shown in Figure 12, with a compilation of the fitted parameters shown in Table 1. Qualitatively, the perturbation functions obtained for wild-type and C102S CmtR<sup>Mtb</sup> are quite similar. However, a quantitative analysis of the data reveals clear differences, the major one being that just one NQI is required to satisfactorily fit the wild-type data, whereas two NQIs are required to satisfactorily fit the C102S perturbation function (Table 1). The high frequency spread (embodied in the  $\Delta\omega_0/\omega_0$  term) of one of the two NQIs in C102S CmtR<sup>Mtb</sup> may cause the amplitude of this signal to be overestimated, but is immaterial to our conclusions. All three NQIs are quite similar and the frequencies are relatively high, indicating the presence of cysteines in the first coordination sphere. PAC parameters  $\omega_0$  and  $\eta$  have been calculated for selected model structures using the semiempirical BASIL method and are compiled in Table 2 (54). A comparison of the observed  $\omega_0$  and  $\eta$  for wild-type and C102S CmtR<sup>Mtb</sup> with those derived from model complexes reveals that a trigonal pyramidal coordination geometry with three coordinating cysteines and distorted tetrahedral coordination geometries of the Cys<sub>3</sub>-H<sub>2</sub>O or Cys<sub>2</sub>-(H<sub>2</sub>O)<sub>2</sub> type are all consistent with the experimental data; however, there are coordination complexes that are not adequately described by this semiempirical model (55). Despite this, the values of  $\omega_0$  (Table 1 and 2) reveal that both tetrahedral Cys<sub>4</sub> and trigonal planar Cys<sub>3</sub> cadmium structures are incompatible with the data (49, 56).

The qualitative similarity of the spectra for the wild-type and C102S CmtR<sup>Mtb</sup> suggest that Cys102, if coordinated, has only a weak interaction with the cadmium ion in the free protein. Thus, a complex formed by Cys57, Cys61, and possibly Cys102 as a



**FIGURE 12:**  $^{111}\text{mCd}$  PAC spectra of wild-type (WT) (*top*) and C102S (*bottom*) CmtR<sup>Mtb</sup>. (A) Experimentally determined perturbation function with error bars (*gray*) with nonlinear least squares fit (*bold faced, black line*) (see Materials and Methods). (B) Fourier transformations of the experimental perturbation function (*thin line*), and fitted function (*bold-faced line*). The first five points of the perturbation function are shown without their associated error bars, to indicate that they are not included in the fit. The parameters from these fits are compiled in Table 1.

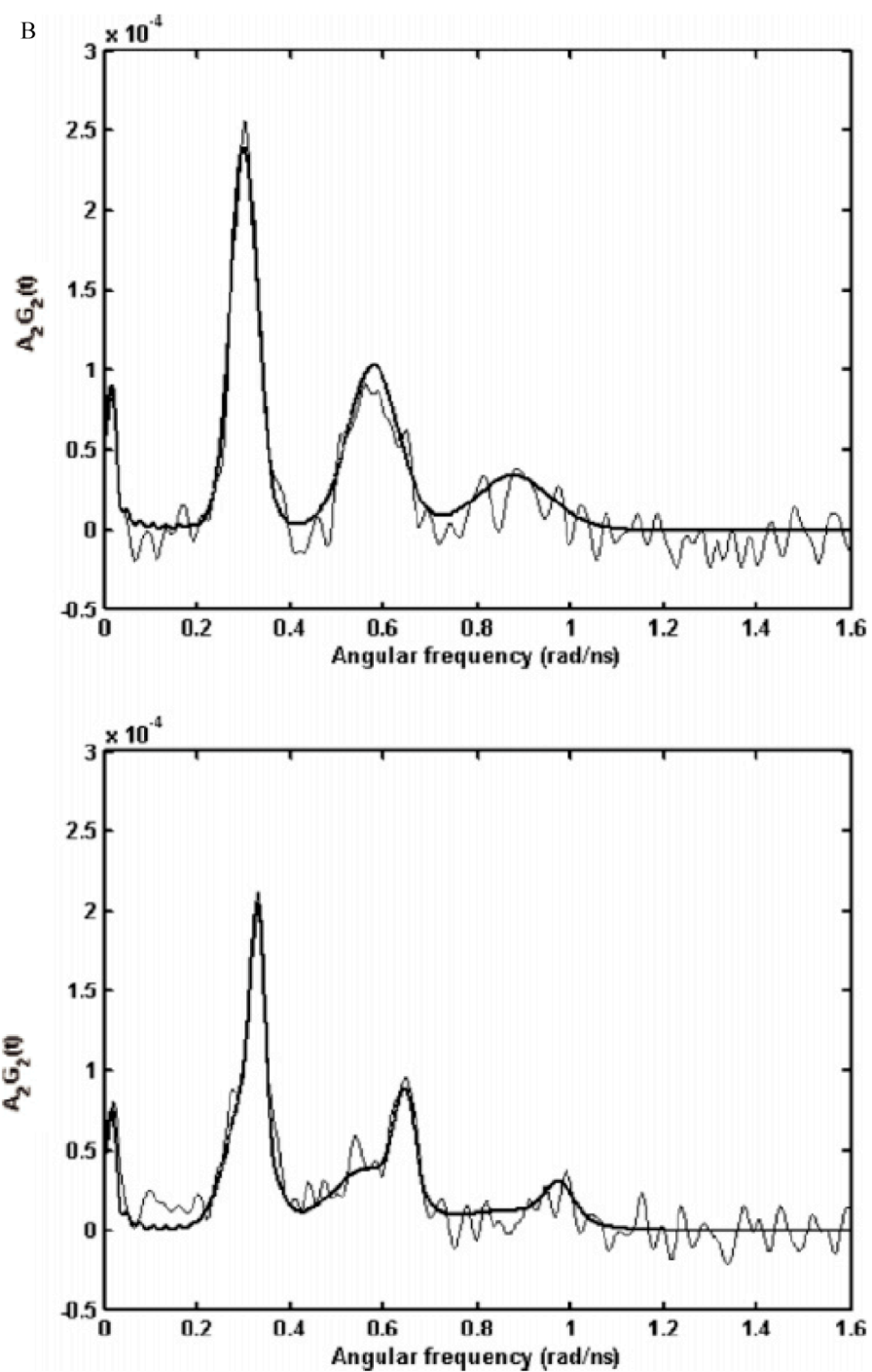


FIGURE 12 continued.



**TABLE 1:** Fitted parameters derived from the  $^{111}\text{mCd}$  perturbed angular correlation spectra (see Fig. 12) obtained for wild-type and C102S CmtR<sup>Mtb</sup>.

Protein	pH	$\omega_0$ (rad/ns)	$\Delta\omega_0/\omega_0$ $\times 100$	$\tau_0$ (ns)	A $\times 100$	$\chi_r^2$	
Wild-type	7.0	0.291 (1) <sup>a</sup>	0.18 (1)	9.0 (4)	323 (42)	7.4 (3)	1.00
C102S	6.7	0.324 (1) 0.285 (7)	0.13 (2) 0.27(3)	3.0 (5) 14 (1)	303 (46)	2.1 (3) 3.8 (4)	1.15

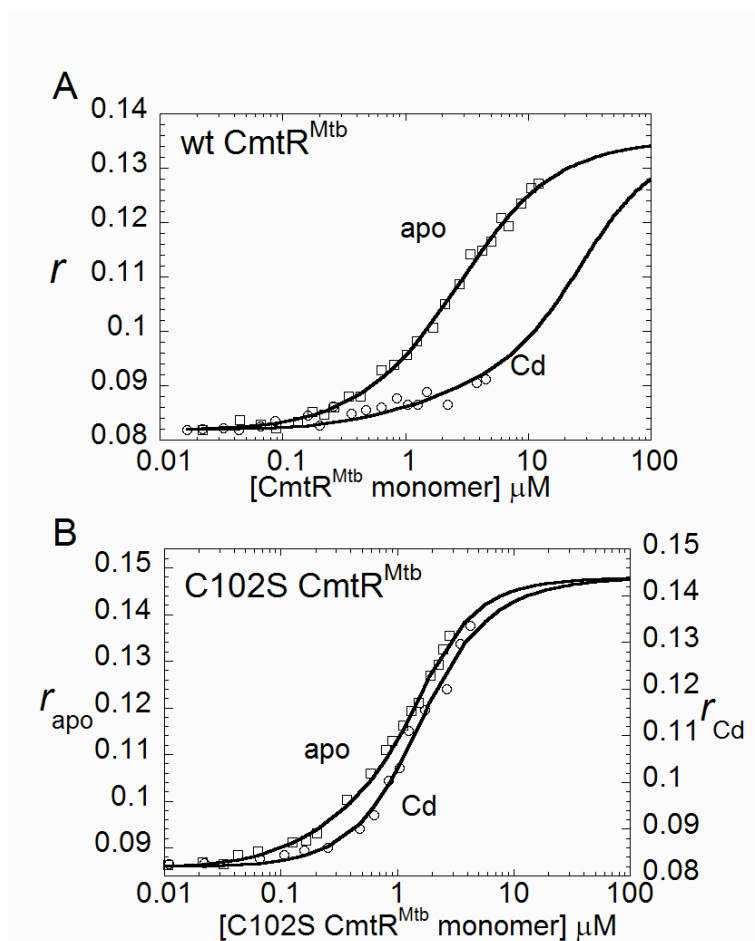
<sup>a</sup>The numbers in parenthesis represent the standard deviation in the last digit of the fitted parameters.

**TABLE 2:** Calculated PAC parameters for model coordination complexes derived from the semi-empirical BASIL method (54).

Coordination sphere	Model structure	$\omega_0$ (rad/ns)	
$[\text{Cd}(\text{Cys})_4]^{2-}$	Tetrahedral	0.000	Not defined
$[\text{Cd}(\text{Cys})_3]^{1-}$	Trigonal planar	0.450	0.00
$[\text{Cd}(\text{Cys})_3]^{1-}$	Trigonal pyramidal	0.300	0.00
$[\text{Cd}(\text{Cys})_3\text{H}_2\text{O}]^{1-}$	Tetrahedral	0.093	0.00
$[\text{Cd}(\text{Cys})_3\text{H}_2\text{O}]^{1-}$	Distorted Tetrahedral <sup>a</sup>	0.261	0.23
$[\text{Cd}(\text{Cys})_2(\text{H}_2\text{O})_2]$	Tetrahedral	0.093	1.00
$[\text{Cd}(\text{Cys})_2(\text{H}_2\text{O})_2]$	Distorted Tetrahedral <sup>b</sup>	0.276	0.33

<sup>a</sup>The S-Cd-S angle increased from 109.47 to 125 degrees for the two of the cysteines.

<sup>b</sup>The S-Cd-S angle increased from 109.47 to 135 degrees.



**FIGURE 13:** Representative *cmt* O/P binding by wild-type (A) and C102S(B) CmtR<sup>Mtb</sup> as monitored by fluorescence anisotropy. A 40-bp 5'-fluorescein-labeled oligonucleotide containing the *cmt* O/P was used for these experiments. Conditions: 10 mM HEPES, 0.4 M NaCl, 1 mM DTT, 50 μM EDTA (for apoprotein titrations) (□) or 10 μM Cd<sup>II</sup> (in Cd-CmtR<sup>Mtb</sup> titrations) (○), pH 7.0. The solid line through each set of data represents the best fit of anisotropy data to a dissociable dimer model assuming 3:1 dimer:DNA complex with  $K_{\text{dimer}}$  fixed at  $1.7 \times 10^7 \text{ M}^{-1}$  for wild-type CmtR<sup>Mtb</sup> and C102S CmtR<sup>Mtb</sup>. The following parameters were obtained: (A) apo wild-type CmtR<sup>Mtb</sup>,  $K_1 = 7.9 (\pm 1.8) \times 10^6 \text{ M}^{-1}$ ,  $K_2 = 1.3 (\pm 0.2) \times 10^6 \text{ M}^{-1}$ ,  $K_3 = 4.5 (\pm 0.5) \times 10^5 \text{ M}^{-1}$ ; Cd-CmtR<sup>Mtb</sup>,  $K_1 = 1.6 (\pm 0.3) \times 10^6 \text{ M}^{-1}$ ,  $K_2 = K_3 \leq 8 \times 10^4 \text{ M}^{-1}$  (upper limit) (B) apo-C102S CmtR<sup>Mtb</sup>,  $K_1 = 1.2 (\pm 0.2) \times 10^7 \text{ M}^{-1}$ ,  $K_2 = 0.9 (\pm 0.3) \times 10^6 \text{ M}^{-1}$ ,  $K_3 = 2.6 (\pm 0.7) \times 10^6 \text{ M}^{-1}$ ; Cd-C102S CmtR<sup>Mtb</sup>,  $K_1 = 2.7 (\pm 1.1) \times 10^6 \text{ M}^{-1}$ ,  $K_2 = 1.7 (\pm 0.9) \times 10^6 \text{ M}^{-1}$ ,  $K_3 = 1.2 (\pm 0.4) \times 10^6 \text{ M}^{-1}$ .

weakly bound ligand and another nonthiolate protein-derived ligand or molecule from the solvent ( $\text{Cl}^-$  or  $\text{H}_2\text{O}$ ) seems most consistent with all the data (see the Discussion). Clearly however, substitution of Cys102 with Ser increases the heterogeneity of the metal coordination sphere with two or more structurally distinct complexes, indicating a role for Cys102 is stabilization of the metal-binding site structure in wild-type  $\text{CmtR}^{\text{Mtb}}$  (Figure 8-10). The fact that two coordination geometries are detected by PAC spectroscopy for C102S  $\text{CmtR}^{\text{Mtb}}$  demonstrates that they are in slow exchange on the  $^{113}\text{Cd}$  NMR time scale ( $\approx \mu\text{s}$ ), and this could explain our inability to observe a  $^{113}\text{Cd}$  resonance for C102S  $\text{CmtR}^{\text{Mtb}}$  (*vide supra*). The relatively low values of  $\eta$  obtained for all metal structures (Table 1) are indicative of coordination geometries only slightly distorted from axial symmetry.

*Allosteric negative regulation of cmt O/P binding by  $\text{Cd}^{II}$  ions.* Previously published gel mobility shift experiments proposed that a 10-5-10 hyphenated inverted repeat in the *cmt* O/P is the regulatory binding site for  $\text{CmtR}^{\text{Mtb}}$  (18). However, these data provided no information on the  $\text{CmtR}^{\text{Mtb}}$ -DNA binding stoichiometry or affinity in the presence and absence of bound metal ions. We therefore designed a fluorescein-labeled 40 base pair duplex oligonucleotide that encompasses the full imperfect 10-5-10 repeat (18) and monitored the binding of wild-type and C102S  $\text{CmtR}^{\text{Mtb}}$ s by measuring changes in the anisotropy of the fluorescein fluorescence of the labeled DNA (20, 22, 23, 26, 29).

Figure 13 shows representative binding isotherms obtained for wild-type  $\text{CmtR}^{\text{Mtb}}$  (Figure 13A) and C102S  $\text{CmtR}^{\text{Mtb}}$  (Figure 13B) in the presence ( $10 \mu\text{M CdCl}_2$ )

and absence (50  $\mu\text{M}$  EDTA) of saturating  $\text{Cd}^{\text{II}}$  at pH 7.0, 0.40 M NaCl, 25°C, solution conditions identical to the analytical ultracentrifugation and metal binding experiments described above. The solid line through each data set represents nonlinear least-squares fit to a sequential dissociable dimer binding model (see Materials and Methods). The magnitude of the change in anisotropy reveals that both  $\text{CmtR}^{\text{Mtb}}$  and C102S  $\text{CmtR}^{\text{Mtb}}$  oligomerize on the DNA and form 1:1, 2:1 and 3:1 protein dimer-DNA complexes, similar to that previously observed for CzrA and SmtB (20, 26). The binding affinities obtained for apo- $\text{CmtR}^{\text{Mtb}}$  are  $K_1 = 7.9 (\pm 1.8) \times 10^6 \text{ M}^{-1}$ ,  $K_2 = 1.3 (\pm 0.2) \times 10^6 \text{ M}^{-1}$  and  $K_3 = 4.5 (\pm 0.5) \times 10^5 \text{ M}^{-1}$  (Figure 13A). Although these values reflect relatively weak DNA binding affinity relative to CadC under the same solution conditions (20, 22), the binding is specific since  $\text{CmtR}^{\text{Mtb}}$  shows no binding to the *nmt* O/P DNA fragment up to a monomer concentration of 10  $\mu\text{M}$  (data not shown).

Furthermore,  $\text{Cd}^{\text{II}}$  negatively allosterically regulates wild-type  $\text{CmtR}^{\text{Mtb}}$  *cmt* O/P binding, reducing the binding affinity of the first dimer by  $\approx 5$ -fold,  $K_1 = 1.6 (\pm 0.3) \times 10^6 \text{ M}^{-1}$ , while eliminating detectable formation of the 2:1 and 3:1 protein-DNA complexes up to 10  $\mu\text{M}$  monomer concentration ( $K_2$  and  $K_3 \leq 8 \times 10^4 \text{ M}^{-1}$ ).

As expected, apo-C102S  $\text{CmtR}^{\text{Mtb}}$  behaves much like apo-wild-type  $\text{CmtR}^{\text{Mtb}}$  and is characterized by *cmt* O/P binding affinities of  $K_1 = 1.2 (\pm 0.2) \times 10^7 \text{ M}^{-1}$ ,  $K_2 = 0.9 (\pm 0.3) \times 10^6 \text{ M}^{-1}$  and  $K_3 = 2.6 (\pm 0.7) \times 10^6 \text{ M}^{-1}$  (Figure 13B). In contrast, the binding isotherm for  $\text{Cd}^{\text{II}}$ -saturated C102S  $\text{CmtR}^{\text{Mtb}}$  is different from that of  $\text{Cd}^{\text{II}}$ -substituted wild-type  $\text{CmtR}^{\text{Mtb}}$  (Figure 13A), with C102S  $\text{CmtR}^{\text{Mtb}}$  still capable of forming 1:1, 2:1 and 3:1 complexes. Resolution of the binding parameters gives  $K_1 = 2.7 (\pm 1.1) \times 10^6 \text{ M}^{-1}$

<sup>1</sup>,  $K_2 = 1.7 (\pm 0.9) \times 10^6 \text{ M}^{-1}$  and  $K_3 = 1.2 (\pm 0.4) \times 10^6 \text{ M}^{-1}$ . These findings reveal that  $\text{Cd}^{\text{II}}$  is fully capable of allosterically negatively regulating the binding of the first C102S CmtR<sup>Mtb</sup> homodimer to DNA to an extent indistinguishable from wild-type CmtR<sup>Mtb</sup> ( $\Delta G_c \approx 1.0 \text{ kcal mol}^{-1}$ ) (Table 3). In contrast,  $\text{Cd}^{\text{II}}$  has little effect on the formation of higher order complexes formed by C102S CmtR<sup>Mtb</sup> on the DNA (compare the last two columns, Table 3). The same trends in allostery are also observed with  $\text{Zn}^{\text{II}}$  (Table 3) and  $\text{Pb}^{\text{II}}$  (data not shown). These results show that Cys102 functions as a key allosteric regulatory ligand, consistent with *in vivo* experiments that showed that C102S CmtR<sup>Mtb</sup>-regulated reporter gene expression is unresponsive to  $\text{Cd}^{\text{II}}$  addition (18). However, they reveal that C102S CmtR<sup>Mtb</sup> is refractory to the metal-mediated disassembly of 2:1 and 3:1 CmtR<sup>Mtb</sup> homodimer:DNA higher order complexes, rather than at the first dimer binding step as observed for other SmtB/ArsR metalloregulators (20, 22, 26). They further argue that the minimal functional repressing complex *in vivo* is a 2:1 CmtR<sup>Mtb</sup> dimer:DNA complex.

## Discussion

*Multiple sequence alignment with other SmtB/ArsR family proteins.* The Cavet and Robinson groups (18) previously established that *M. tuberculosis* CmtR<sup>Mtb</sup> contained  $\text{Cd}^{\text{II}}/\text{Pb}^{\text{II}}$  sensing sites that must be structurally distinct from previously well-characterized  $\alpha 3\text{N}$  and  $\alpha 5$  sites in SmtB/ArsR sensors. A multiple sequence alignment (Figure 5B) shows that *M. tuberculosis* CmtR<sup>Mtb</sup> (18), a previously characterized  $\text{Hg}^{\text{II}}$  sensor *S. lividans* MerR (57), and putative homologs in other actinomycetes have just three conserved Cys, corresponding to Cys57, Cys61 and Cys102 in *M. tuberculosis*

**TABLE 3:** Summary of  $K_i$  obtained for the binding of apo, Cd<sup>II</sup>-substituted and Zn<sup>II</sup>-substituted wild-type and C102S CmtR<sup>Mtb</sup> to *cmt* O/P DNA<sup>a</sup>

		$K_1$ $\times 10^6 M^{-1}$	$K_2$ $\times 10^6 M^{-1}$	$K_3$ $\times 10^6 M^{-1}$	${}^b\Delta G_1$ kcal mol <sup>-1</sup>	$\sum\Delta G$ kcal mol <sup>-1</sup>	$\Delta G_c$ kcal mol <sup>-1</sup>	${}^d\Delta G_c^{\sum G}$ kcal mol <sup>-1</sup>
CmtR <sup>Mtb</sup>	Apo	$6.8 \pm 1.9$	$1.4 \pm 0.3$	$0.6 \pm 0.1$	-9.3	-25.5	—	—
	Cd	$1.4 \pm 0.3$	$\leq 0.08$	$\leq 0.08$	-8.3	-21.7	1.0	$\geq 3.8$
	Zn	$1.0 \pm 0.2$	$\leq 0.08$	$\leq 0.08$	-8.1	-21.4	1.2	$\geq 4.1$
C102S CmtR <sup>Mtb</sup>	Apo	$11.1 \pm 1.9$	$1.2 \pm 0.4$	$2.2 \pm 0.5$	-9.6	-26.4	—	—
	Cd	$3.0 \pm 0.9$	$1.6 \pm 0.8$	$1.1 \pm 0.3$	-8.8	-25.4	0.8	1.0
	Zn	$2.1 \pm 0.7$	$0.4 \pm 0.2$	$1.0 \pm 0.4$	-8.6	-24.3	1.0	2.1

<sup>aa</sup> $K_i$  reflects the mean of  $K_i \pm$  std error determined from 2-3 independent experiments.

<sup>b</sup> $\Delta G_l = -RT \ln K$  (T = 298K), <sup>c</sup> $\Delta G_c = \Delta G_{l \text{ metal}} - \Delta G_{l \text{ apo}}$ , <sup>d</sup> $\Delta G_c^{\sum G} = \sum \Delta G_{\text{metal}} - \sum \Delta G_{\text{apo}}$

CmtR<sup>Mtb</sup> and completely lack the cysteine residues that comprise the well-characterized  $\alpha$ 3N Cd<sup>II</sup>/Pb<sup>II</sup> sensing sites found in CadCs (22, 23, 29, 39). Indeed, we have purified a CmtR<sup>Mtb</sup> homolog from *Streptomyces coelicolor* A3(2) (NP\_627722) (see Figure 5B) and have shown that the Pb<sup>II</sup> absorption spectrum is indistinguishable from that of *M. tuberculosis* CmtR<sup>Mtb</sup> (See chapter IV). How do the Cd<sup>II</sup> and Pb<sup>II</sup> binding properties of these two classes of heavy metal sensing sites compare?

*Comparative metal binding properties of CmtR<sup>Mtb</sup> and pI258 CadC.* In general, the binding of the first Cd<sup>II</sup> or Pb<sup>II</sup> ion to the CmtR<sup>Mtb</sup> homodimer occurs with an affinity that is within an order of magnitude of  $K_{Cd}$  and  $K_{Pb}$  for CadC (22). The greatest difference in fact has to do with the extent of negative cooperativity of metal binding, which appears to be far greater for CmtR<sup>Mtb</sup> vs. CadC (22); in fact, binding of a second Pb<sup>II</sup> ion to the CmtR<sup>Mtb</sup> homodimer could not be observed under these experimental conditions (Figure 9), a finding formally consistent with “half-the-sites reactivity” (58-60). Interestingly, the Hg<sup>II</sup> regulator, MerR, binds a single Hg<sup>II</sup> ion per dimer (61), and is sufficient to allosterically induce underwinding/bending (62) of the *mer* operator/promoter. Likewise, a single Pb<sup>II</sup> ion per CmtR<sup>Mtb</sup> dimer appears necessary and sufficient to allosterically regulate *cmt* O/P binding to the full extent (Figure 13). This is in contrast to what has been reported for CadC (63).

The first coordination shells are clearly different as well. Previous spectroscopic studies of CadC are consistent with a strongly distorted  $S_4$  or  $S_3O$  Cd<sup>II</sup> complex and a trigonal  $S_3$  Pb<sup>II</sup> complex (22, 29). The Cd<sup>II</sup> and Pb<sup>II</sup> chelates of CmtR<sup>Mtb</sup> are generally indicative of lower molar absorptivities and, in the case of the Pb<sup>II</sup>



spectrum, a significant blue-shift, relative to the  $\text{Cd}^{\text{II}}$  and  $\text{Pb}^{\text{II}}$  complexes formed by CadC (22, 29). These data collectively suggest that  $\text{CmtR}^{\text{Mtb}}$  has one fewer strongly bound thiolate ligand, a result consistent with the  $^{113}\text{Cd}$  NMR resonance frequencies obtained for  $\text{CmtR}^{\text{Mtb}}$  ( $\delta=480$  ppm) vs. CadC ( $\delta=622$  ppm) (22). This result alone would seem to rule out direct metal coordination by Cys102 in the free protein, although the  $\text{Cd}^{\text{II}}$  optical titration data and a comparison of the  $K_{\text{Me}}$  for wild-type and C102S  $\text{CmtR}^{\text{Mtb}}$ s (Figures 7-9) would seem to argue against this. Cys102 might be analogous to Cys11 in *S. aureus* pI258 CadC, which has been argued to be a weakly bound, or weakly deshielding (of the  $^{113}\text{Cd}$  nucleus) thiol(ate) ligand (29, 64). In contrast to Cys11 in CadC however, Cys102 in  $\text{CmtR}^{\text{Mtb}}$  is a key allosteric ligand (*vide infra*).

The coordination number ( $n$ ) of the metal complex in  $\text{CmtR}^{\text{Mtb}}$  is clearly three as revealed by perturbed angular correlation (PAC) spectroscopy of the  $^{111\text{m}}\text{Cd}^{\text{II}}$ -substituted  $\text{CmtR}^{\text{Mtb}}$  (Figure 12; Table 1). This feature distinguishes  $\text{CmtR}^{\text{Mtb}}$  from CadC, which adopts a distorted tetrahedral complex; recent PAC experiments of  $^{111\text{m}}\text{Cd}$ -substituted CadC are consistent with this interpretation (X. Chen, L. Hemmingsen, R. Bauer and D. Giedroc, manuscript in preparation). PAC spectroscopy of wild-type vs. C102S  $\text{CmtR}^{\text{Mtb}}$  do not unambiguously reveal if Cys102 is a first shell ligand in the free protein since both spectra are quite similar; however, substitution of Cys102 with a nonliganding Ser side chain clearly increases the structural heterogeneity of the metal complex.  $\text{Pb}^{\text{II}}$  EXAFS, like that previously done for CadC (29), will also be required to unambiguously determine the number of thiolate donor atoms in the  $\text{Pb}^{\text{II}}$  coordination complexes of  $\text{Pb}^{\text{II}}$ -substituted wild-type and C102S  $\text{CmtR}^{\text{Mtb}}$ . It is worth noting that the

Co<sup>II</sup> UV-Vis absorption spectrum of Co<sup>II</sup>-CmtR<sup>Mtb</sup> is quite unusual (18) (data not shown) but similar (albeit slightly blue-shifted), to that of *L. monocytogenes* CadC (29), with at least three well-resolved low intensity ligand-field transitions ( $\lambda = 530, 675$  and  $760$  nm); this spectrum suggests a strongly distorted Co<sup>II</sup> complex.

Although the biological data are limited, some CadCs mediate metalloregulation of gene expression by Zn<sup>II</sup> in addition to more thiophilic ions Cd<sup>II</sup> and Pb<sup>II</sup>; in the case of *S. aureus* pI258 CadC, zinc resistance via derepression of the *cad* operon (which encodes genes for both CadC and CadA, a P-type ATPase) is robust in *E. coli* that lack the major zinc resistance system encoded by the *znt* operon (32). Interestingly, induction of the *cmt* operon in *M. smegmatis* is reported to be selective for Cd<sup>II</sup> and Pb<sup>II</sup>, with no induction mediated by Zn<sup>II</sup>, at least at the concentrations tested (18). Our original thought was that perhaps CmtR<sup>Mtb</sup> bound Zn<sup>II</sup> weakly by virtue of forming a lower coordination number ( $n=3$ ) complex, since Zn<sup>II</sup> shows a strong preference for four-coordinate complexes or higher. This proved not to be the case, since the binding affinity of the first Zn<sup>II</sup> to CmtR<sup>Mtb</sup> is quite high ( $K_{Zn1} \approx 10^{10} \text{ M}^{-1}$ ) (Figure 10). Nonetheless, this is lower than estimates of  $K_{Zn}$  for pI258 CadC by at least an order of magnitude, and far lower than that determined for *bona fide* SmtB/ArsR Zn<sup>II</sup> sensors SmtB (19, 25) and CzrA (30). In any case, Zn<sup>II</sup> is an effective allosteric regulator of CmtR<sup>Mtb</sup>-*cmt* O/P binding equilibria *in vitro* (Figure 13), and is in fact indistinguishable from Cd<sup>II</sup> and Pb<sup>II</sup> in this assay. Previous studies with other SmtB/ArsR sensors reveal that coordination geometry is a major determinant for metal selectivity (20) (M. Pennella and D. Giedroc, submitted for publication); thus, Zn<sup>II</sup> may adopt a metal complex that is

isostructural with that of the  $\text{Pb}^{\text{II}}$  and  $\text{Cd}^{\text{II}}$  complexes.

Why then is  $\text{Zn}^{\text{II}}$  a non-inducer *in vivo*? One possibility is that  $\text{Zn}^{\text{II}}$  fluxes in *M. smegmatis* simply don't reach the levels sufficient to induce the *cmt* operon *in vivo*, relative to toxic heavy metals  $\text{Cd}^{\text{II}}$  and  $\text{Pb}^{\text{II}}$ . Alternatively, there are differences in the extent to which biologically essential  $\text{Zn}^{\text{II}}$  is trafficked or made bioavailable in *M. smegmatis*. Indeed, previous work from the Robinson laboratory reveals that *M. smegmatis* does not accumulate  $\text{Zn}^{\text{II}}$  when cultured in media containing maximally permissive concentrations of  $\text{Zn}^{\text{II}}$  salts (27); thus, it is not surprising that  $\text{CmtR}^{\text{Mtb}}$  does not sense  $\text{Zn}^{\text{II}}$  in *M. smegmatis*. It would be of interest to determine if *cmt* expression could be induced in a cyanobacterial cell, where  $\text{Zn}^{\text{II}}$  pools are clearly sufficient to be detected by known high affinity zinc sensor, *Synechococcus* SmtB (27). These findings also partly explain why  $\text{Zn}^{\text{II}}$  is a non-inducer of the  $\text{Ni}^{\text{II}}/\text{Co}^{\text{II}}$ -responsive *nmt* operon in *M. smegmatis*, which encodes the  $\text{Ni}^{\text{II}}/\text{Co}^{\text{II}}$  sensing SmtB/ArsR repressor, NmtR (27); however, in this case,  $\text{Zn}^{\text{II}}$  is poorer allosteric inducer *in vitro* as well, relative to  $\text{Ni}^{\text{II}}$  and  $\text{Co}^{\text{II}}$ , because it fails to adopt the proper coordination geometry in the regulatory active sites (20).

*How do metal ions induce negative allosteric regulation of  $\text{CmtR}^{\text{Mtb}}$  binding to the *cmt* O/P?* Quantitative fluorescence anisotropy-based DNA binding experiments analyzed with a multiple-dimer binding model reveal that all metal ions tested,  $\text{Cd}^{\text{II}}$ ,  $\text{Pb}^{\text{II}}$  and  $\text{Zn}^{\text{II}}$ , lower the binding affinity of all  $\text{CmtR}^{\text{Mtb}}$  homodimers for the *cmt* O/P, with the effect greatest on the formation of higher order (2:1 and 3:1) complexes, which are not observed under these conditions (Figure 13, Table 3). Stated another way, inducing

metals regulate the assembly, and therefore mediate the disassembly, of an oligomeric protein-DNA complex. Strikingly, substitution of Cys102 with a nonliganding Ser essentially abrogates metalloregulation of the assembly of 2:1 and 3:1 complexes, with little influence on the binding of the first dimer. These features are novel relative to other SmtB/ArsR family metalloregulators, where the binding of inducing metal ions lowers the affinity of the first dimer by 300-10,000-fold, giving an allosteric coupling free energy,  $\Delta G_c$  of  $\approx +3$  to  $\geq +5$  kcal mol<sup>-1</sup> (25 °C) (20, 22, 26) (M. Pennella and D. Giedroc, submitted for publication). In the case of CmtR,  $\Delta G_c$  is small,  $\leq 1.0$  kcal mol<sup>-1</sup>, and is not appreciably affected by substitution of this key allosteric ligand (Table 3). One intriguing possibility is that the C-terminal Cys102 (see Figure 5A) mediates the formation metal-crosslinked tetramers on the DNA, with Cys102 from one dimer forming a metal coordination bond to the opposite dimer; formation of this metal-liganding tetramer might significantly lower CmtR<sup>Mtb</sup> binding affinity. This possibility remains to be tested. In any case, Cys102 in CmtR<sup>Mtb</sup> is functionally analogous to allosteric ligands Cys7 and Cys60 in *S. aureus* pI258 CadC, mutagenesis of which significantly reduces (Cys7) or completely abrogates (Cys60) Cd<sup>II</sup>/Pb<sup>II</sup>-mediated metalloregulation of *cad* O/P binding (29).

When our data are taken together, they suggest a “division of labor” within the metal sensing chelate of CmtR<sup>Mtb</sup>. Cys57 and Cys61, at the C-terminus of the proposed  $\alpha 4$  helix (Figure 5A), anchor the metal coordination complex; replacement of either of these two residues with nonliganding residues is expected to greatly diminish metal binding affinity, consistent with the lack of a metal response for C57S and C61S

CmtR<sup>Mtb</sup>s *in vivo* (18). Remarkably, metal binding to the Cys57/Cys61 pair in CmtR<sup>Mtb</sup> occurs in exactly the same region of the protein that is coupled to the interhelical  $\alpha 5$  Zn<sup>II</sup> sites in the zinc sensors SmtB and CzrA, via an intersubunit hydrogen-bonding network (30). However, metal coordination by the Cys57/Cys61 pair is necessary but not sufficient since Cys102, while playing a comparatively minor role in stabilizing the chelate in the uncomplexed protein, is required to fully mediate allosteric coupling of metal and *cmt* O/P binding (Figure 9); this explains the inducer non-responsiveness of C102S CmtR<sup>Mtb</sup> in *M. smegmatis* (18).

*Possible biological function of CmtR<sup>Mtb</sup>.* The biological function of CmtR<sup>Mtb</sup> in *M. tuberculosis* is not yet known. However, CmtA exhibits very high sequence similarity to the well characterized P<sub>1B</sub>-type heavy metal transporting ATPases from *E. coli* (ZntA) as well as *S. aureus* (CadA). *E. coli* ZntA is capable of effluxing Cd<sup>II</sup>, Pb<sup>II</sup> and Zn<sup>II</sup> (32, 33, 65, 66) and its expression is metalloregulated by the MerR family regulator ZntR (67). Although Zn<sup>II</sup> was the first metal ion inducer identified for ZntA (67), Cd<sup>II</sup> and Pb<sup>II</sup> were subsequently shown to upregulate *ZntA* expression as well (66); in fact, one analysis of the metal inducibility profile of *ZntA-lacZ* fusion constructs revealed that Cd<sup>II</sup> was the most potent inducer, relative to Zn<sup>II</sup> and Pb<sup>II</sup> in *E. coli* (66). A similar metal specificity profile appears to characterize *S. aureus* CadA as well, whose expression is regulated by the SmtB/ArsR family regulator CadC in response to Cd<sup>II</sup>, Pb<sup>II</sup> and to a lesser extent Zn<sup>II</sup> (68). This leads us to propose that *M. tuberculosis* CmtA will have similar metal exporting properties as ZntA and CadA. Why *M. tuberculosis* encodes the *cmt* operon is unknown, since this opportunistic pathogen is unlikely to

encounter Cd<sup>II</sup>/Pb<sup>II</sup> toxicity during the course of its life cycle. It remains to be determined whether this operon is regulated by other stress responses *in vivo*.

Finally, it is striking to note that three distinct metalloregulators, the MerR family regulator ZntR, and two structurally distinct SmtB/ArsR regulators CadC and CmtR<sup>Mtb</sup>, all regulate the expression of essentially the same P-type ATPase efflux pump in response to the same overlapping set of divalent metal ions. This suggests a “mix and match” approach in the evolution of heavy metal resistance systems (sensor plus resistance genes) of defined metal selectivities, perhaps mediated by the recently documented lateral transfer of genes encoding P<sub>IB</sub>-type ATPase efflux pumps among subsurface bacterial species (69).

## Conclusion

We establish that both wild-type and C102S CmtR<sup>Mtb</sup>s are homodimeric in solution under experimental conditions. It can bind Cd<sup>II</sup>, Pb<sup>II</sup> and Zn<sup>II</sup> tightly via formation of cysteine thiolate coordination bonds with an apparent metal binding stoichiometry of 0.5-1.0 per protomer, which is in contrast to previous findings (18). C102S CmtR<sup>Mtb</sup> binds Cd<sup>II</sup> and Zn<sup>II</sup> with only a slightly lower affinity relative to wild-type CmtR ( $\approx$  10~20 fold), and 100~1000 fold lower in Pb<sup>II</sup> binding. Results from UV-Vis optical spectroscopy, <sup>113</sup>Cd NMR spectroscopy and <sup>111m</sup>Cd PAC spectroscopy suggest that the coordination complex is anchored by two strong thiolate donor atoms, proposed to be Cys57 and Cys61, while Cys102 appears to make a smaller but measurable contribution to the LMCT<sup>1</sup> intensity in the ultraviolet. The *cmt* O/P binding affinity of apo-wild-type and apo-C102S CmtR<sup>Mtb</sup> are similar but Cd<sup>II</sup> strongly negative

regulates the assembly of high order (2:1, 3:1) wild-type CmtR<sup>Mtb</sup> homodimer:*cmt* O/P complexes, but not those formed by C102S CmtR<sup>Mtb</sup>. In summary, Cys102, while making a minor contribution to metal binding affinity, is critically required for allosteric negative regulation of *cmt* O/P binding.

CHAPTER IV  
METAL BINDING PROPERTIES OF A PUTATIVE CmtR HOMOLOG  
ENCODED BY *S. coelicolor* A3(2)

### **Introduction**

*Streptomyces* are soil-dwelling, filamentous Gram-positive bacteria belonging to the taxonomy order of *Actinomycetales* (70, 71). This genus is distinguished for its complex multicellular development and biologically active production of secondary metabolites. (71). Over two-thirds of naturally derived antibiotics in use today are produced by *Streptomyces* (71). *Streptomyces coelicolor* A3(2) is the genetically best defined *Streptomyces* strain and has become the model organism. The complete genome sequence was published in 2002 and it is among the largest fully sequenced prokaryotic genomes. It has a 8.67 Mb linear chromosome with 72.12% G+C content and is particularly rich in regulatory proteins (12.3% from 7825 predicted genes) (71, 72). Some subsets of regulatory proteins are particularly prevalent by this genome, e.g.  $\sigma$  factors (71).

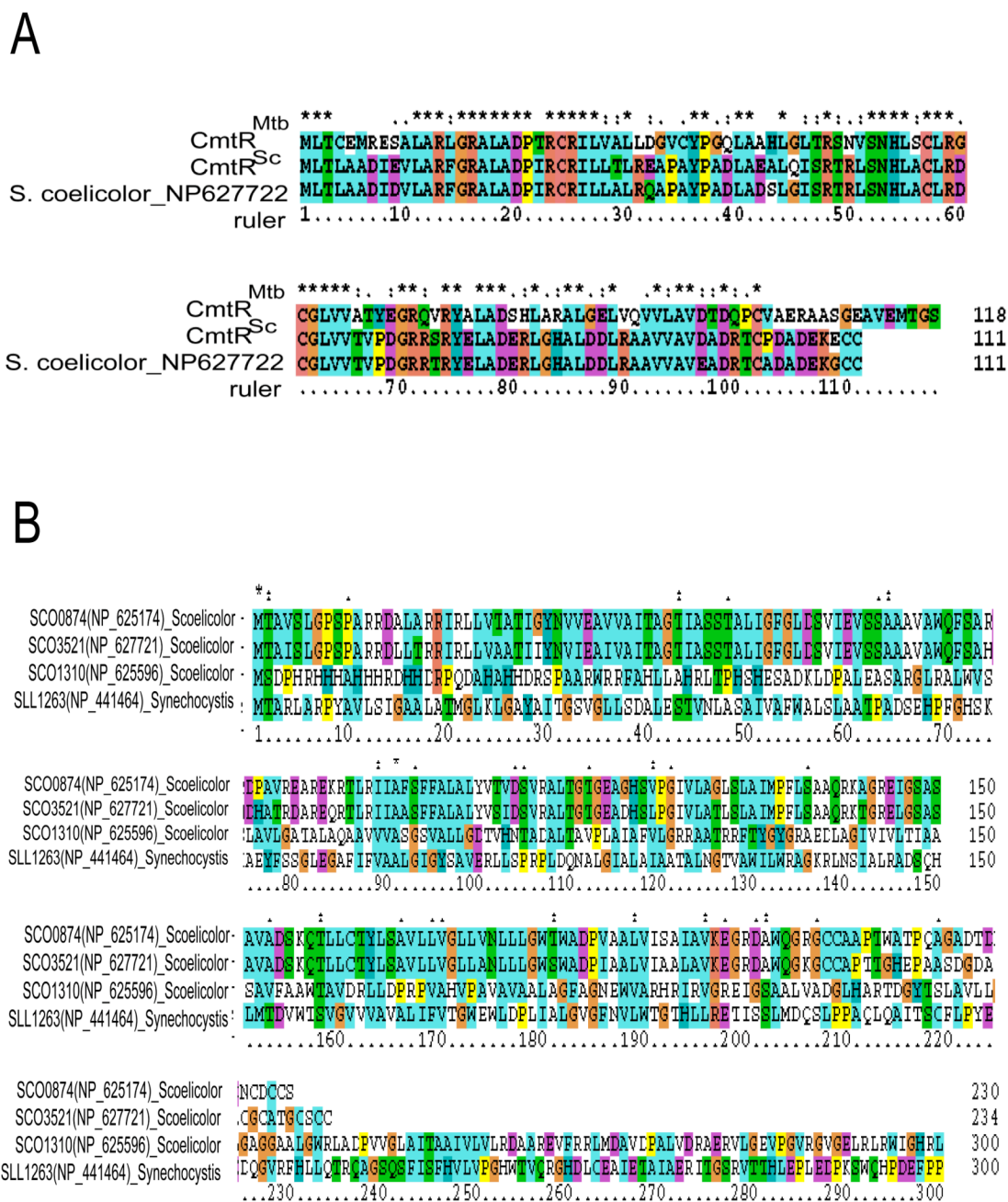
Living in a complex and variable environment as soil, *S. coelicolor* has developed a sophisticated mechanism to overcome different stresses (71). For example, temperature and osmotic upshifts can transiently induce a set of  $\sigma$  factors, anti- $\sigma$  factors and anti- $\sigma$  factor antagonists to prepare *S. coelicolor* for multiple stresses (73). Bacterial  $\sigma$  factors is an essential component of RNA polymerase (RNAP) (74). They selectively direct gene sets transcription by binding to the RNAP core enzyme and affecting its



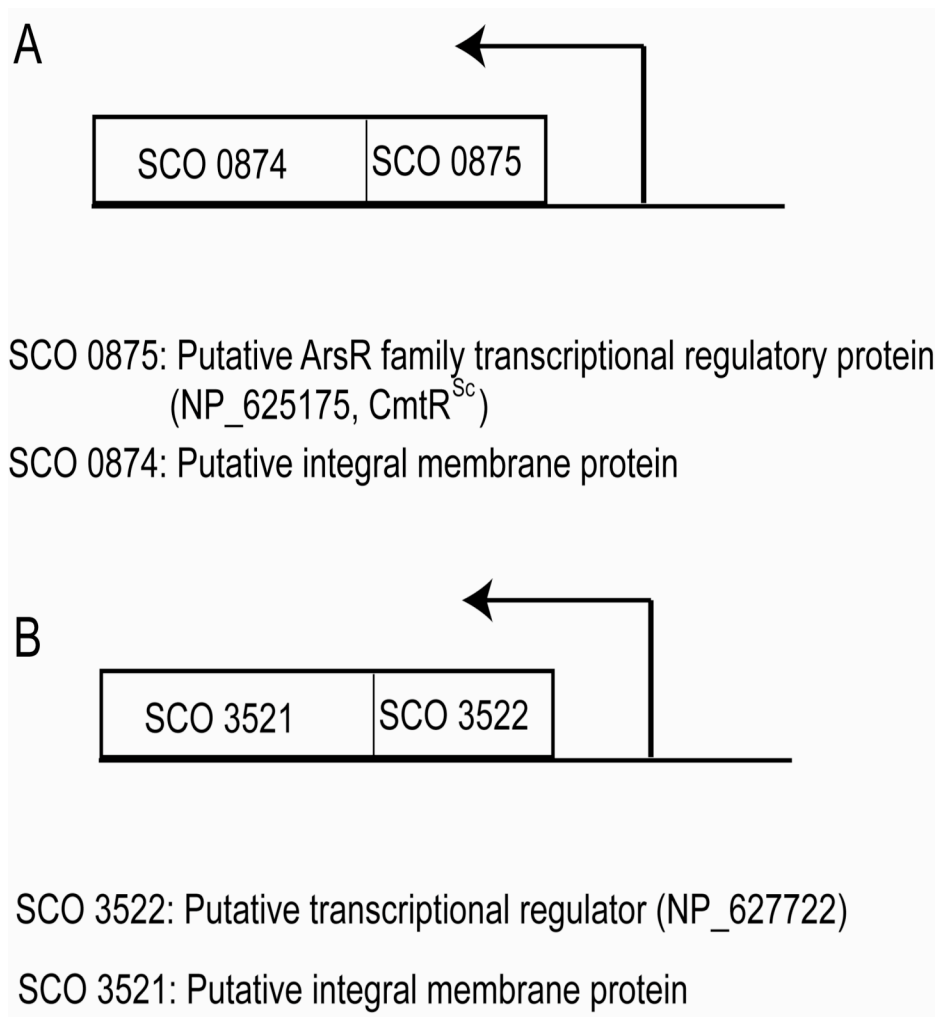
promoter specificity (71). *S. coelicolor* has 65  $\sigma$  factors which is the largest number in all sequenced bacterial genomes (71), 45 of which belongs to ECF (extra-cytoplasmic function)  $\sigma$  factors. (71). Upon external stimuli, ECF  $\sigma$  factors activate genes involved in disulphide stress, cell-wall homeostasis and aerial mycelium development (71). Most ECF  $\sigma$  factors's availability can be regulated by one or more cotranscribed negative regulators, which include a transmembrane protein functioning as an anti- $\sigma$  factor that binds, and inhibits, the cognate  $\sigma$  factor(71, 74). A recently characterized anti-sigma factor RsrA selectively binds sigma factor  $\sigma^R$  in response to redox changes in the environment, via a thiol-disulfide exchange process. (75) Stoichiometric  $Zn^{II}$  can help thiol-reduced RsrA to retain a structure favorable for  $\sigma^R$  binding (75).

A search for protein homologs for *M. tuberculosis* CmtR<sup>Mtb</sup> by blastp returns two hits in *S. coelicolor* A3(2): NP\_627722 and NP\_625175. The proteins represent just two of the 14 predicted ArsR/SmtB regulators encoded by *S. coelicolor*. The two proteins encoded by these genes differ from each other in just ten amino acids, and each shares  $\approx 50\%$  identity with *M. tuberculosis* CmtR<sup>Mtb</sup>, including four key cysteines from a total of six. These cysteines correspond to the residue positions Cys24, Cys57, Cys61 and Cys102 in *M. tuberculosis* CmtR<sup>Mtb</sup> (Figure 14A). For the experiments presented here, we have chosen NP\_625175 for detailed study and have designated it CmtR<sup>Sc</sup>.

NP\_625175 is a putative SmtB/ArsR family transcriptional regulatory protein, designated CmtR<sup>Sc</sup> and is encoded by the ORF designated SCO0875. This protein has 52% sequence identity to CmtR<sup>Mtb</sup> and has a putative helix-turn-helix motif situated between residues 35 to 56 (predicted by NCBI). The gene immediately downstream



**FIGURE 14:** Sequence comparison of (A) *M. tuberculosis* CmtR<sup>Mtb</sup> and 2 putative homologs from *S. coelicolor* A3(2) (NP\_62175, designated as CmtR<sup>Sc</sup>, and NP\_627722), (B) SCO0875's immediate downstream gene SCO0874 and its homologs (NP\_627721, NP\_625596, NP\_441464), generated by Clustal X.



**FIGURE 15:** Schematic representations of Cmt<sup>Sc</sup> and the putative SCO3521/SCO3522 operons.

gene of SCO0875 is SCO0874 is a predicted integral membrane protein that has high similarity to cation efflux (CE) or cation diffusion facilitator (CDF) family of integral membrane metal transporters (76). Likewise, NP\_627722 encoded by ORF SCO3522, is positioned immediately downstream of SCO3521, also predicted to be a CDF family member. Together with another two homologs SCO1310 (NP\_625596) in *S. coelicolor* and SLL1263 (NP\_441464) in *Synechocystis*, these proteins have a conserved domain belongs to COG0053, which is a predicted Co<sup>II</sup>/Zn<sup>II</sup>/Cd<sup>II</sup> cation transporters cluster (Figure 14B). The cluster proteins greatly increase tolerance to divalent metal ions, such as Cd<sup>II</sup>, Zn<sup>II</sup>, and Co<sup>II</sup> (77) and Zn<sup>II</sup> and are widespread in eukaryotic cells and plants (78, 79). One example is Cd<sup>II</sup>/Zn<sup>II</sup>/Co<sup>II</sup> transporter CzcD in *E. coli* (80). Although we don't yet know the operator/promotor regions of *cmt<sup>Sc</sup>* operon to which CmtR<sup>Sc</sup> binds, schematic representations of CmtR<sup>Sc</sup> and the putative SCO3521/SCO3522 operons are shown in Figure 15.

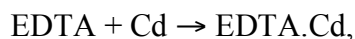
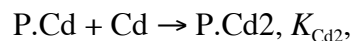
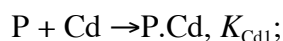
A subset of four cysteine residues in CmtR<sup>Sc</sup> are common with those in CmtR<sup>Mtb</sup>, and three (Cys57, Cys61 and Cys102) are strong candidates for key ligands in metal binding and allosteric regulation (18). As a result, we expected to observe similar metal binding properties of CmtR<sup>Mtb</sup> and CmtR<sup>Sc</sup>. However, there are two neighboring C-terminal cysteine residues in CmtR<sup>Sc</sup>, Cys110 and Cys111, that may also be involved in metal chelating. (Figure 14). Therefore, it was of interest to express CmtR<sup>Sc</sup> and examine its metal binding characteristics *in vitro*, compared to that in CmtR<sup>Mtb</sup>. It seemed possible to us that the cysteines at the extreme C-terminus could influence the Pb<sup>II</sup> and Cd<sup>II</sup> properties, particularly in light of recent results with a ArsR repressor *E.*

*coli* ArsD, where two cysteine pairs (Cys12/Cys13 and Cys112/Cys113) have been shown to facilitate metalloid exchange between sites (81). Therefore, we constructed a double mutant C110G/C111S CmtR<sup>Sc</sup> in which the two C-terminal cysteines of CmtR<sup>Sc</sup> were replaced by amino acids corresponding to the C-terminal residues of CmtR<sup>Mtb</sup>. In this chapter, we describe the results of preliminary Cd<sup>II</sup>/Pb<sup>II</sup>/Zn<sup>II</sup> titration experiments with CmtR<sup>Sc</sup> compared to that of C110G/C111S CmtR<sup>Sc</sup>. We then discuss these results in context of the metal binding sites and selectivities in *M. tuberculosis* CmtR<sup>Mtb</sup> established by previous work (Chapter III).

### Experimental procedures

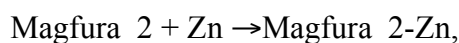
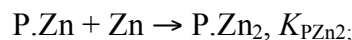
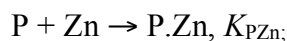
*Cd<sup>II</sup>, Pb<sup>II</sup> optical absorption spectroscopy.* All metal binding experiments were carried out anaerobically at ambient temperature (~25°C) using a Hewlett-Packard model 8452A spectrophotometer (22). For Cd<sup>II</sup> titrations, apoproteins were diluted using final dialysis buffer S to  $\approx 50 \mu\text{M}$  in 800  $\mu\text{L}$  and loaded into an anaerobic cuvette fitted with a Hamilton gas-tight adjustable volume syringe containing 0.5 mM Cd<sup>II</sup> titrant in the glove box. Complete optical spectra of apo protein were collected from 200-900 nm 1-2 min after each addition of a known aliquot (5-15  $\mu\text{L}$ ) of Cd<sup>II</sup>. Corrected spectra were obtained by subtraction of the apoprotein spectra from each spectrum obtained after addition of metal ion, and further corrected for dilution. Pb<sup>II</sup> titrations were done in exactly the same way except that 10 mM bis-tris, 0.4 M NaCl, pH 7.0 was used as the buffer. Bis-Tris is a weakly chelating buffer that can prevent excess Pb<sup>II</sup> from forming Pb<sup>II</sup>(OH)<sub>2</sub> precipitate (44). Cd<sup>II</sup> competition experiment performed with EDTA was carried out as described above except 200-300  $\mu\text{M}$  chelator was present. The

competition binding curves were fit to the model using Dynafit:



where  $K_{Cd-EDTA} = 3.2 \times 10^{12} \text{ M}^{-1}$  under these condition.

*Zn<sup>II</sup> binding experiments.* The zinc chelator dye magfura-2 ( $K_{Zn} = 5.0 \times 10^7 \text{ M}^{-1}$  at pH 7.0 and 25°C) (25) was used as a colorimetric competitor for Zn<sup>II</sup> binding by wild-type CmtR<sup>Sc</sup> as previously described (25). 30  $\mu\text{M}$  wild-type CmtR<sup>Sc</sup> and 14.7  $\mu\text{M}$  magfura-2 were used. The data were fit to a competitive binding model assuming two nonequivalent, noninteractive metal binding sites per CmtR<sup>Sc</sup> protomer by DynaFit:

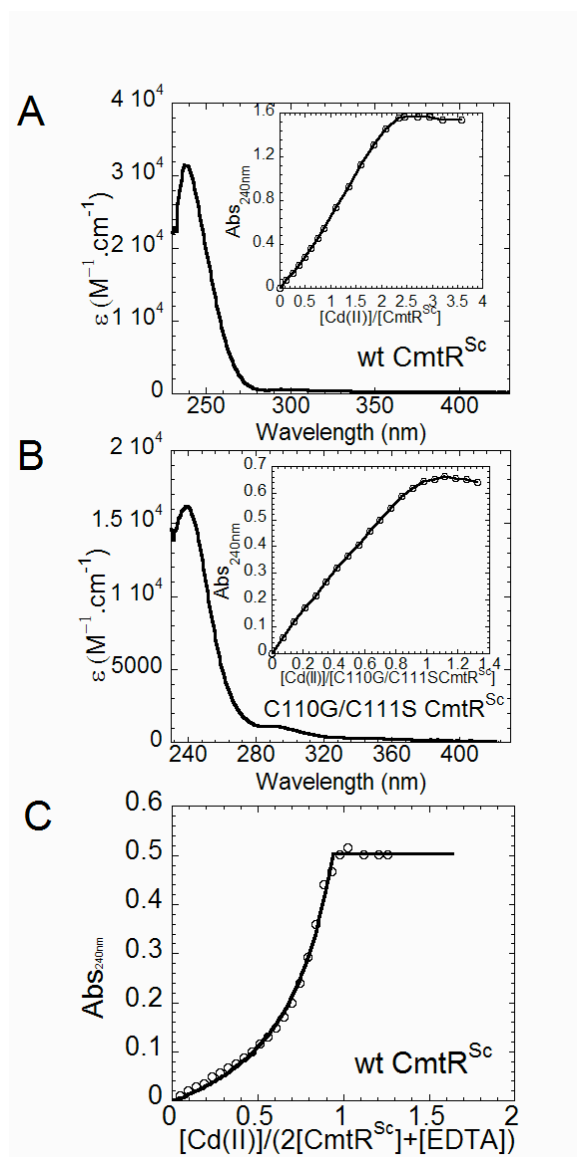


where  $K_{Zn-magfura2} = 5.0 \times 10^7 \text{ M}^{-1}$  under these conditions..

## Results and discussion

Wild-type and C110G/C111S CmtR<sup>Sc</sup> were purified to homogeneity and subjected to free thiol determination as discussed in Material and Methods (Chapter II). Wild-type CmtR<sup>Sc</sup> was nearly fully reduced (5.8 cysteines of 6.0 expected) with C110G/C111S CmtR<sup>Sc</sup> contained 3.0 out of 4.0.

*Cd<sup>II</sup> optical spectroscopy.* Apoprotein-subtracted Cd<sup>II</sup> absorbance spectra of wild-type and C110G/C111S CmtR<sup>Sc</sup> are shown in Figure 16. The saturated Cd<sup>II</sup> spectra



**FIGURE 16:** Apo-subtracted difference spectrum of Cd<sup>II</sup>-saturated (A) apo wild-type CmtR<sup>Sc</sup> (50.7 μM), (B) apo C110G/C111S CmtR<sup>Sc</sup> (44.8 μM). CmtR<sup>Sc</sup> variants were titrated anaerobically with increasing concentrations of Cd<sup>II</sup>. Inset, Cd<sup>II</sup> binding isotherm plotted a change in A<sub>240</sub> vs. [CmtR<sup>Sc</sup> variant monomer] (C) Cd<sup>II</sup>-EDTA competition binding isotherm in which 20.9 μM wt CmtR<sup>Sc</sup> was titrated with Cd<sup>II</sup> in presence of 227 μM EDTA. Conditions: 10 mM HEPES, 0.4 M NaCl, pH 7.0, 25°C.

of both proteins are characterized by an intense ligand-to-metal charge transfer at 240nm, similar to that observed with CmtR<sup>Mtb</sup>. Binding isotherms (*insets*) were obtained by plotting the corrected absorbance at 240 nm as a function of total [Cd<sup>II</sup>] over protein monomer ratio. The maximum molar absorptivity at 240 nm for CmtR<sup>Sc</sup> is  $\approx 31,000 \text{ M}^{-1} \text{ cm}^{-1}$  which is essential twice of wild-type CmtR<sup>Mtb</sup> ( $\epsilon \approx 16,000 \text{ M}^{-1} \text{ cm}^{-1}$ ) (Figure 16A). Consistent with this, wild-type CmtR<sup>Sc</sup> exhibits a 2:1 binding stoichiometry (Figure 16A), which is also twice that of CmtR<sup>Mtb</sup>. From the shape of binding isotherm, two Cd<sup>II</sup> ions bind CmtR<sup>Sc</sup> monomer appear to be slightly positively cooperative binding (Figure 16A).

Strikingly, C110G/C111S CmtR<sup>Sc</sup> double mutant is characterized by a similar Cd<sup>II</sup> saturation curve as wild-type CmtR<sup>Mtb</sup> with molar absorptivities  $\approx 16,000 \text{ M}^{-1} \text{ cm}^{-1}$  (Figure 16B), or exactly one half that of wild-type CmtR<sup>Sc</sup>. Consistent with this, the mutant binds  $\sim 0.9$  molar equivalent of Cd<sup>II</sup> or near approximately one half fold of CmtR<sup>Sc</sup> (Figure 16B). This is close to 1:1, but suggests that some fraction of two metal binding sites in the dimer are inactivated, likely due to cysteine oxidation. The same was found for CmtR<sup>Mtb</sup> (Chapter III). Direct metal to protein titration experiments like those shown in Figure 16A and B can only present a lower limit for binding affinity constant  $K_{\text{Cd}}$ . Therefore, the same Cd<sup>II</sup> titration experiment was performed in presence of  $20.9 \mu\text{M}$  wild-type CmtR<sup>Sc</sup> and  $227 \mu\text{M}$  EDTA (Figure 15C), with  $K_{\text{Cd-EDTA}} = 3.2 \times 10^{12} \text{ M}^{-1}$  under solution conditions. A nonlinear least square fit of a simple competition model assuming two non-equivalent, non-interacting sites per protomer gives  $K_{\text{Cd1}} = (1.2 \pm 0.1) \times 10^{12} \text{ M}^{-1}$ ,  $K_{\text{Cd2}} = (1.4 \pm 0.4) \times 10^{11} \text{ M}^{-1}$ . Interestingly,  $K_{\text{Cd}}$  for CmtR<sup>Mtb</sup>



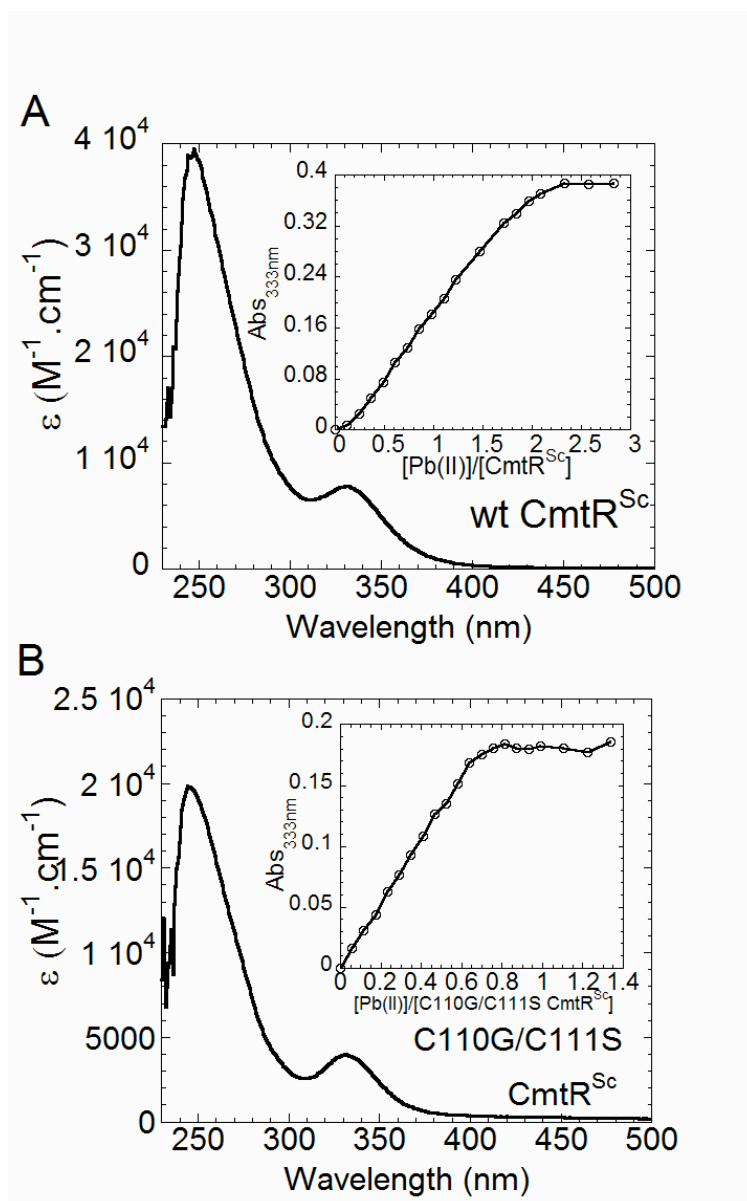
determined under the same solution condition is  $1.7 \times 10^{12} \text{ M}^{-1}$ , which is very close to  $K_{\text{CdI}}$  for CmtR<sup>Sc</sup>.

These results suggest that CmtR<sup>Sc</sup> has two pairs spectroscopically similar metal sites per per homodimer, which differ in macroscopic affinity by  $\approx 10$  fold. Previous results with CmtR<sup>Mtb</sup> reveal that Cys 57, Cys 61 and Cys 102 were ligands to Cd<sup>II</sup> in wild-type CmtR (18), although Cys102 seems to play only a minor role in metal ion stabilization. These three cysteines probably constitute one of the Cd<sup>II</sup> sites in CmtR<sup>Sc</sup> as in CmtR<sup>Mtb</sup> and the three different cysteines in CmtR<sup>Sc</sup> forming the other site.

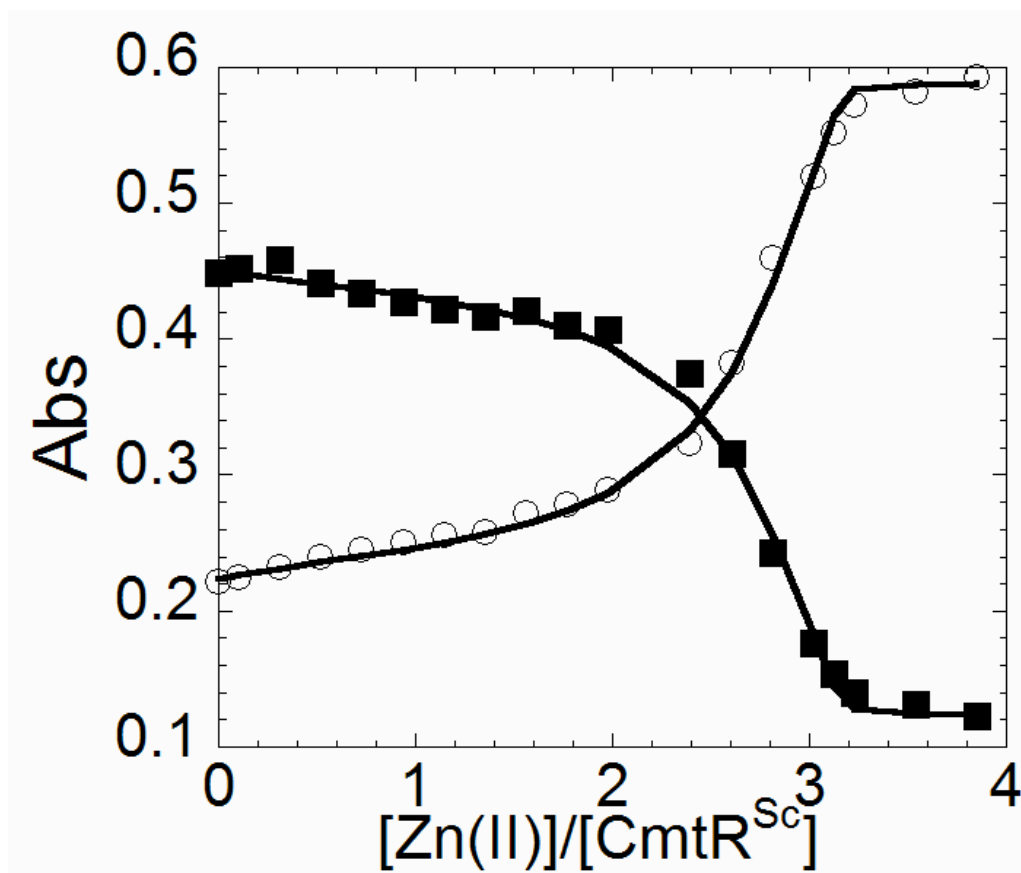
*Pb<sup>II</sup> optical spectroscopy.* Apoprotein-subtracted difference spectrum of Pb<sup>II</sup>-saturated wild-type and C110G/C111S CmtR<sup>Sc</sup> are shown in Figure 17. Anaerobic Pb<sup>II</sup> titration experiments were performed under  $\approx 50 \mu\text{M}$  apo-wild-type CmtR<sup>Sc</sup> (Figure 17A) and C110G/C111S CmtR<sup>Sc</sup> (Figure. 17B). The saturated Pb<sup>II</sup> spectra of both proteins are characterized by an intense absorption in the far-ultraviolet and a long-wavelength absorption band with maximum at 333 nm, which are the same as what we observed in CmtR<sup>Mtb</sup>. Binding isotherms (*insets*) were obtained by plotting the corrected absorbance at 333 nm as a function of total [Pb<sup>II</sup>]/protein monomer ratio. For wild-type CmtR<sup>Sc</sup>, Pb<sup>II</sup> binding exhibits  $\approx 2:1$  ratio over [CmtR<sup>Sc</sup>] monomer as Cd<sup>II</sup> binding, with an apparent slightly positive cooperative binding isotherm (Figure 17A). This ratio drops to  $\approx 0.7$  Pb<sup>II</sup>/protein monomer for C110G/C111S CmtR<sup>Sc</sup>. (Figure 17B). The maximum molar absorptivity at 333 nm for wild-type CmtR<sup>Sc</sup> is  $\approx 7800 \text{ M}^{-1} \text{ cm}^{-1}$  which is similar as CmtR<sup>Mtb</sup> ( $\epsilon_{333} = 7900 \text{ M}^{-1} \text{ cm}^{-1}$ ) (Figure 17A). This drops to  $\approx 3950 \text{ M}^{-1} \text{ cm}^{-1}$  for C110G/C111S CmtR<sup>Sc</sup> (Figure 17B), which is only half of CmtR<sup>Mtb</sup>.

An intriguing fact is the molar absorptivity differences at 333 nm for CmtR<sup>Sc</sup> variants. CmtR<sup>Sc</sup> was revealed to have two times Cd<sup>II</sup>-S bonds of CmtR<sup>Mtb</sup> in Cd<sup>II</sup> titration experiment based on 2 folds molar absorptivities in CmtR<sup>Sc</sup> of CmtR<sup>Mtb</sup>, because  $\epsilon$  is an indication of metal-S bonds amounts (50, 51). Therefore, we can know CmtR<sup>Sc</sup> has equal number of Pb<sup>II</sup>-S bonds as CmtR<sup>Mtb</sup> from Pb<sup>II</sup> titration experiments. However, this conclusion is contradicted to the fact of  $\approx 2:1$  CmtR<sup>Sc</sup>/metal ratio for both Cd<sup>II</sup> and Pb<sup>II</sup> ions. But if we measure the maximum Pb<sup>II</sup> binding absorbance directly, CmtR<sup>Sc</sup> is still two-times of CmtR<sup>Mtb</sup> (Figure 9A and Figure 17A). What is the reason for 50% molar absorptivity drop down in Pb<sup>II</sup>-CmtR<sup>Sc</sup>? One possibility is we supposed 50% active protein concentration when calculated molar absorptivity in CmtR<sup>Mtb</sup>-Pb<sup>II</sup> based on the 0.5 Pb<sup>II</sup> binding stoichiometry, which increases molar absorptivities by two fold in CmtR<sup>Mtb</sup>. Another possibility is the maximum molar absorptivities can not reflect actual amounts of Pb<sup>II</sup>-S bonds in this example. This discrepancy needs to be clarified in future.

The absorption spectrum similarities between CmtR<sup>Sc</sup> and CmtR<sup>Mtb</sup> suggest formation of Pb<sup>II</sup>-thiolate complexes with similar coordination geometry. The nonintegral binding stoichiometry in C110G/C111S CmtR<sup>Sc</sup> suggests partial inactivation of Pb<sup>II</sup> binding site. Another possibility is that Cd<sup>II</sup> binding in CmtR<sup>Sc</sup> involves in different cysteine ligands as Pb<sup>II</sup>, considering the stoichiometry differences between these two metal ions in C110G/C111S CmtR<sup>Sc</sup> (Figure 16B, Figure 17B). Predicted by blastp, CmtR<sup>Sc</sup>'s downstream gene SCO0874 is a Cd<sup>II</sup>/Zn<sup>II</sup>/Co<sup>II</sup> efflux protein, which does not include Pb<sup>II</sup>. If it is true, the Cd<sup>II</sup>/Pb<sup>II</sup> binding sites differentiation in CmtR<sup>Sc</sup> may



**FIGURE 17:** Apo-subtracted difference spectrum of Pb<sup>II</sup>-saturated apo (A) wild-type CmtR<sup>Sc</sup> (50.8  $\mu$ M), (B) C110G/C111S CmtR<sup>Sc</sup> (53.7  $\mu$ M). CmtR<sup>Sc</sup> variants were titrated anaerobically with increasing concentrations of Cd<sup>II</sup>. *Inset*, Pb<sup>II</sup> binding isotherm plotted a change in  $A_{333}$  vs. [CmtR<sup>Sc</sup> variant monomer] Conditions: 10 mM Bis-tris, 0.4 M NaCl, pH 7.0, 25°C.



**FIGURE 18:** Representative titrations of  $\text{Zn}^{\text{II}}$  into a mixture of mag-fura-2 and wild-type  $\text{CmtR}^{\text{Sc}}$ .  $30 \mu\text{M}$   $\text{CmtR}^{\text{Sc}}$  and  $14.7 \mu\text{M}$  mag-fura-2 were present. The empty circles represent  $A_{325}$  and the filled squares represent  $A_{366}$ . The solid line represents a global non-linear least square fit to a model that incorporates the stepwise binding of two  $\text{Zn}^{\text{II}}$  (defined by  $K_{\text{pZn}}$  and  $K_{\text{pZn}2}$ ) to a  $\text{CmtR}^{\text{Sc}}$  monomer using Dynafit. The following parameters were obtained:  $K_{\text{pZn}} = 5.3 (\pm 1.8) \times 10^8 \text{ M}^{-1}$  (a lower limit under these conditions),  $K_{\text{pZn}2} = 6.7 (\pm 1.4) \times 10^8 \text{ M}^{-1}$ . Conditions: 10 mM HEPES and 0.4 M NaCl at pH 7.0 and  $25^\circ\text{C}$ .

contribute to selectively response to  $\text{Cd}^{\text{II}}$  but not  $\text{Pb}^{\text{II}}$  in  $\text{cmt}^{\text{Sc}}$  operon as  $\text{Zn}^{\text{II}}$  to NmtR(20). Further evidence are needed to prove the biological function of SCO0874.  $\text{Cmt}^{\text{Sc}}$  operator/promoter region is also need to be mapped. Thus we can use in vitro methods to examine the metal binding effeto allosteric negative regulation.

*$\text{Zn}^{\text{II}}$  binding affinities obtained via chelator competition experiments with magfura-2.* Zinc indicator dye magfura-2 ( $K_{\text{Zn}\cdot\text{mag-fura-2}} = 5.0 \times 10^7 \text{ M}^{-1}$ ) was used as a competitor of  $\text{Zn}^{\text{II}}$  binding to  $\text{CmtR}^{\text{Sc}}$  in this experiment to determine  $\text{Zn}^{\text{II}}$  binding stoichiometry and affinity constant  $K_{\text{Zn}}$  (25). Figure 18 shows representative titrations of  $\text{Zn}^{\text{II}}$  into mixtures of wild-type  $\text{CmtR}^{\text{Sc}}$  and mag-fura-2. The solid curves represent a fit to a model that describes the binding of two successive  $\text{Zn}^{\text{II}}$  ions to the  $\text{CmtR}^{\text{Sc}}$  monomer, considering each monomer-metal binding as an independent event. Estimated parameters from curve fitting are  $K_{\text{PZn}} = 5.3 (\pm 1.8) \times 10^8 \text{ M}^{-1}$ ,  $K_{\text{PZn2}} = 6.7 (\pm 1.4) \times 10^8 \text{ M}^{-1}$  for wild-type  $\text{CmtR}^{\text{Sc}}$ , which are identical to one another within experimental error. This  $\text{Zn}^{\text{II}}$  site in  $\text{CmtR}^{\text{Sc}}$  is different from  $\text{CmtR}^{\text{Mtb}}$ , which exhibits a negative cooperativity within the dimer with one site in  $\sim 10^{10} \text{ M}^{-1}$  range and the other in  $\sim 10^5 \text{ M}^{-1}$ .

Future experiments need to be done to examine  $\text{CmtR}^{\text{Sc}}$  assembly states, monitor  $\text{Co}^{\text{II}}$  binding, map  $\text{cmt}^{\text{Sc}}$  operator/promoter region, explore the biological function of downstream gene SCO0874 and measure allosteric regulation of  $\text{CmtR}^{\text{Sc}}$ - $\text{cmt}^{\text{Sc}}$  operator/promoter complex formation

## CHAPTER V

### SUMMARY AND PERSPECTIVE

*Mycobacterium tuberculosis* CmtR<sup>Mtb</sup> is a Cd<sup>II</sup>/Pb<sup>II</sup> sensing SmtB/ArsR family member with novel metal binding sites. (18). It is structurally distinct from both the nickel-cobalt SmtB/ArsR family protein NmtR found in the same organism (27) as well as *Staphylococcus aureus* pI258 CadC (18) that possesses both  $\alpha$ 3N and  $\alpha$ 5 sites and has the same biological function (39). *In vivo*  $\beta$ -galactosidase assays carried in *M. smegmatis* revealed CmtR<sup>Mtb</sup> can metalloregulate reporter gene expression in presence of Cd<sup>II</sup> and Pb<sup>II</sup> salts but not Zn<sup>II</sup>. Of the six cysteine residues, Cys57, Cys61 and Cys102 are proved to be important in CmtR<sup>Mtb</sup> heavy metal sensing (18). Detailed *in vitro* characterization of CmtR<sup>Mtb</sup> is required to better understand its metalloregulation mechanism, including the metal binding affinity, stoichiometry, coordination chemistry and metal mediated allosteric regulation of binding with *cmt*<sup>Mtb</sup> O/P region. We focused our attention on Cys102 in the C-terminal region of CmtR<sup>Mtb</sup> and the molecular basis for metalloregulation of DNA binding

Experimental results reveal that both homodimeric CmtR<sup>Mtb</sup> and C102S CmtR<sup>Mtb</sup> capable binding Cd<sup>II</sup>, Pb<sup>II</sup> and Zn<sup>II</sup> via formation of cysteine thiolate coordination bonds with an apparent metal-binding stoichiometry of 0.5~1. Metal binding affinity constants determined by UV-Vis optical spectroscopy reveal that Cys102 does not play a critical role in Cd<sup>II</sup> and Zn<sup>II</sup> binding but have more influence in Pb<sup>II</sup>. <sup>113</sup>Cd NMR spectroscopy ( $\epsilon = 480$  ppm) and spectras in <sup>111m</sup>Cd PAC spectroscopy suggest the coordination complex is anchored by two strong thiolate donor atoms Cys57 and Cys61, while

Cys102 makes a smaller but measurable contribution to the LMCT intensity in the ultraviolet. Fluorescence anisotropy reveals Cys102 contributes to the strongly negative regulation of higher order (2:1, 3:1) CmtR<sup>Mtb</sup> homodimer/*cmt* O/P complex assembly. In other words, Cys102, although making a minor contribution to metal-binding affinity, is critically required for allosteric regulation of *cmt* O/P binding.

A long-term goal is to determine to which extent the structure at functionally important regulatory metal sites can be predicted on the basis of amino acid sequence alone. *S. coelicolor* A3(2) is a soil bacterium that contains 14 SmtB/ArsR family members (16). A putative homolog encoded by *S. coelicolor* (CmtR<sup>Sc</sup>) has four cysteine residues in common with *M. tuberculosis* CmtR (CmtR<sup>Mtb</sup>), including Cys24, Cys57, Cys61 and Cys102, as well as two additional C-terminal cysteines Cys110, Cys111 (Figure 14). These structural similarities and differences between CmtR<sup>Mtb</sup> and CmtR<sup>Sc</sup> provide us with a great opportunity to investigate influence of these cysteines in metal binding.

We make the striking finding that CmtR<sup>Sc</sup> binds two metals per protomer, or twice that of CmtR<sup>Mtb</sup>. Furthermore, one of the binding site is destroyed by mutagenesis of the C-terminal cysteine pairs in C110G/C111S CmtR<sup>Sc</sup>. What are the structures of the two metal sites? One possibility is that one site exactly corresponds to CmtR<sup>Mtb</sup>, while the other site perhaps includes Cys24, Cys110 and Cys111. It would be interesting to know the role of individual cysteine in every putative site.

What is the biological function of SCO0875, which is down-stream gene of CmtR<sup>Sc</sup> (SCO0874)? Is it a Cd<sup>II</sup>/Co<sup>II</sup>/Zn<sup>II</sup> efflux protein as predicted by homology

modelling? Traditional  $\beta$ -Galactosidase assay and metal sensitivity assays can be used to answer this question directly by measuring reporter gene expression under a variety of metal ion stimuli (18, 82). We can also directly monitor the metal induced gene expression by real time quantitative RT-PCR (83) and microarray (82). These methods can provide a clear functional context for our in vitro results.

CmtR<sup>Mtb</sup> and CmtR<sup>Sc</sup> were found in different species, but the high similarity between these two proteins lead us to believe they probably evolve from a common ancestor. The two organisms *M. tuberculosis* and *S. coelicolor* A3(2), are actually quite closely related to one other. The *M. tuberculosis* complex, composed of *M. tuberculosis*, *M. bovis*, *M. bovis* BCG, *M. africanum* and *M. microti* is believed to have evolved from a progenitor developed from a soil bacterium (17). Today *S. coelicolor* A3(2) may well be a representative of the group of soil-dwelling filamentous bacteria since it belongs to the same taxonomic order (*Actinomycetales*) as *M. tuberculosis* and *M. leprae* (71). As SmtB/ArsR family proteins are present in archaea, bacteria and eubacteria, these proteins might have evolved before the archaea and bacteria split (16). On the other hand, it is possible that many horizontal gene transfer and lineage-specific gene losses occurs among organisms during evolution (16). Many important structural features have been identified and characterized throughout SmtB/ArsR protein family, eg, the thiophilic  $\alpha$ 3N and  $\alpha$ 5 metal binding sites (10). The discovery of *M. tuberculosis* CmtR and a putative homolog in *S. coelicolor* A3(2), provides a third example of a structurally distinct sensing site in SmtB/ArsR proteins. This finding can potentially increase our understanding of the rules governing metal ion selectivity and metal site design.



In conclusion, the SmtB/ArsR family Cd<sup>II</sup>/Pb<sup>II</sup> sensor *M. tuberculosis* CmtR binds Cd<sup>II</sup>, Pb<sup>II</sup> and Zn<sup>II</sup> tightly via cysteine thiolate coordination bonds with an apparent metal-binding stoichiometries of 0.5-1 per protomer or 1~2 per dimer. The metal binding ligands have distinct functions. Cys57 and Cys61 anchor the metal coordination complex, while Cys102 plays a comparatively minor role in stabilizing the metal chelate but is required to fully mediate allosteric coupling of metal and *cmt* O/P binding. Characterization of a putative homolog of CmtR<sup>Mtb</sup>, designated CmtR<sup>Sc</sup> from *S. coelicolor* A3(2) reveals that this protein possesses one additional metal binding site per protomer than CmtR<sup>Mtb</sup> but with similar metal sites structures. Characterization of double mutant C110G/C111S CmtR<sup>Sc</sup> reveals one of the two metal binding sites is lost in CmtR<sup>Sc</sup>, resulting in a protein with apparent similar metal binding characteristics as CmtR<sup>Mtb</sup>. It will be interesting to determine both metal sites in CmtR<sup>Sc</sup> are required for metalloregulation of *cmt*<sup>Sc</sup> O/P binding. Finally, our studies of CmtR<sup>Sc</sup> represent the first step in discovery of ArsR/SmtB sensors with novel ligand specifications.

## REFERENCES

1. Finney, L. A., and O'Halloran, T. V. (2003) Transition metal speciation in the cell: insights from the chemistry of metal ion receptors. *Science* 300, 931-936
2. Rosen, D. R. (1993) Mutations in Cu/Zn superoxide dismutase gene are associated with familial amyotrophic lateral sclerosis. *Nature* 364, 362
3. Vulpe, C., Levinson, B., Whitney, S., Packman, S., and Gitschier, J. (1993) Isolation of a candidate gene for Menkes disease and evidence that it encodes a copper-transporting ATPase. *Nat Genet* 3, 7-13
4. Mercer, J. F., Livingston, J., Hall, B., Paynter, J. A., Begy, C., Chandrasekharappa, S., Lockhart, P., Grimes, A., Bhave, M., Siemieniak, D., and et al. (1993) Isolation of a partial candidate gene for Menkes disease by positional cloning. *Nat Genet* 3, 20-25
5. Bull, P. C., Thomas, G. R., Rommens, J. M., Forbes, J. R., and Cox, D. W. (1993) The Wilson disease gene is a putative copper transporting P-type ATPase similar to the Menkes gene. *Nat Genet* 5, 327-337
6. Rensing, C. (2005) Form and function in metal-dependent transcriptional regulation: dawn of the enlightenment. *J Bacteriol* 187, 3909-3912
7. Wunderli-Ye, H., and Solioz, M. (1999) Copper homeostasis in *Enterococcus hirae*. *Adv Exp Med Biol* 448, 255-264
8. Outten, C. E., and O'Halloran, T. V. (2001) Femtomolar sensitivity of metalloregulatory proteins controlling zinc homeostasis. *Science* 292, 2488-2492
9. Rosen, B. P. (1996) Bacterial resistance to heavy metals and metalloids. *JBIC* 1, 273-277
10. Busenlehner, L. S., Pennella, M. A., and Giedroc, D. P. (2003) The SmtB/ArsR family of metalloregulatory transcriptional repressors: structural insights into prokaryotic metal resistance. *FEMS Microbiol Rev* 27, 131-143
11. Brown, N. L., Stoyanov, J. V., Kidd, S. P., and Hobman, J. L. (2003) The MerR family of transcriptional regulators. *FEMS Microbiol Rev* 27, 145-163
12. Williams, R.J.P., and Fraústo da Silva J. J. R. (1991, 2001) The biological chemistry of the elements: *the inorganic chemistry of life*. OXFORD University

*Express*

13. Moore, C. M., and Helmann, J. D. (2005) Metal ion homeostasis in *Bacillus subtilis*. *Curr Opin Microbiol* 8, 188-195
14. Robinson, N. J., Whitehall, S. K., and Cavet, J. S. (2001) Microbial metallothioneins. *Adv Microb Physiol* 44, 183-213
15. Ralston, D. M., and O'Halloran, T. V. (1990) Ultrasensitivity and heavy-metal selectivity of the allosterically modulated MerR transcription complex. *Proc Natl Acad Sci U S A* 87, 3846-3850
16. Perez-Rueda, E., Collado-Vides, J., and Segovia, L. (2004) Phylogenetic distribution of DNA-binding transcription factors in bacteria and archaea. *Comput Biol Chem* 28, 341-350
17. Cole, S. T., Brosch, R., Parkhill, J., Garnier, T., Churcher, C., Harris, D., Gordon, S. V., Eiglmeier, K., Gas, S., Barry, C. E., 3rd, Tekaiia, F., Badcock, K., Basham, D., Brown, D., Chillingworth, T., Connor, R., Davies, R., Devlin, K., Feltwell, T., Gentles, S., Hamlin, N., Holroyd, S., Hornsby, T., Jagels, K., Krogh, A., McLean, J., Moule, S., Murphy, L., Oliver, K., Osborne, J., Quail, M. A., Rajandream, M. A., Rogers, J., Rutter, S., Seeger, K., Skelton, J., Squares, R., Squares, S., Sulston, J. E., Taylor, K., Whitehead, S., and Barrell, B. G. (1998) Deciphering the biology of *Mycobacterium tuberculosis* from the complete genome sequence. *Nature* 393, 537-544
18. Cavet, J. S., Graham, A. I., Meng, W., and Robinson, N. J. (2003) A cadmium-lead-sensing ArsR-SmtB repressor with novel sensory sites. Complementary metal discrimination by NmtR AND CmtR in a common cytosol. *J Biol Chem* 278, 44560-44566
19. VanZile, M. L., Cospers, N. J., Scott, R. A., and Giedroc, D. P. (2000) The zinc metalloregulatory protein *Synechococcus* PCC7942 SmtB binds a single zinc ion per monomer with high affinity in a tetrahedral coordination geometry. *Biochemistry* 39, 11818-11829
20. Pennella, M. A., Shokes, J. E., Cospers, N. J., Scott, R. A., and Giedroc, D. P. (2003) Structural elements of metal selectivity in metal sensor proteins. *Proc Natl Acad Sci U S A* 100, 3713-3718
21. Liu, T., Nakashima, S., Hirose, K., Shibasaki, M., Katsuhara, M., Ezaki, B., Giedroc, D. P., and Kasamo, K. (2004) A novel cyanobacterial SmtB/ArsR family repressor regulates the expression of a CPx-ATPase and a metallothionein in response to both Cu(I)/Ag(I) and Zn(II)/Cd(II). *J Biol Chem* 279, 17810-17818

22. Busenlehner, L. S., Cosper, N. J., Scott, R. A., Rosen, B. P., Wong, M. D., and Giedroc, D. P. (2001) Spectroscopic properties of the metalloregulatory Cd(II) and Pb(II) sites of *S. aureus* pI258 CadC. *Biochemistry* 40, 4426-4436
23. Busenlehner, L. S., Apuy, J. L., and Giedroc, D. P. (2002) Characterization of a metalloregulatory bismuth(III) site in *Staphylococcus aureus* pI258 CadC repressor. *J Biol Inorg Chem* 7, 551-559
24. Ji, G., and Silver, S. (1992) Regulation and expression of the arsenic resistance operon from *Staphylococcus aureus* plasmid pI258. *J Bacteriol* 174, 3684-3694
25. VanZile, M. L., Chen, X., and Giedroc, D. P. (2002) Structural characterization of distinct alpha3N and alpha5 metal sites in the cyanobacterial zinc sensor SmtB. *Biochemistry* 41, 9765-9775
26. VanZile, M. L., Chen, X., and Giedroc, D. P. (2002) Allosteric negative regulation of smt O/P binding of the zinc sensor, SmtB, by metal ions: a coupled equilibrium analysis. *Biochemistry* 41, 9776-9786
27. Cavet, J. S., Meng, W., Pennella, M. A., Appelhoff, R. J., Giedroc, D. P., and Robinson, N. J. (2002) A nickel-cobalt-sensing ArsR-SmtB family repressor. Contributions of cytosol and effector binding sites to metal selectivity. *J Biol Chem* 277, 38441-38448
28. Thelwell, C., Robinson, N. J., and Turner-Cavet, J. S. (1998) An SmtB-like repressor from *Synechocystis* PCC 6803 regulates a zinc exporter. *Proc Natl Acad Sci U S A* 95, 10728-10733
29. Busenlehner, L. S., Weng, T. C., Penner-Hahn, J. E., and Giedroc, D. P. (2002) Elucidation of primary (alpha(3)N) and vestigial (alpha(5)) heavy metal-binding sites in *Staphylococcus aureus* pI258 CadC: evolutionary implications for metal ion selectivity of ArsR/SmtB metal sensor proteins. *J Mol Biol* 319, 685-701
30. Eicken, C., Pennella, M. A., Chen, X., Koshlap, K. M., VanZile, M. L., Sacchettini, J. C., and Giedroc, D. P. (2003) A metal-ligand-mediated intersubunit allosteric switch in related SmtB/ArsR zinc sensor proteins. *J Mol Biol* 333, 683-695
31. Shi, W., Dong, J., Scott, R. A., Ksenzenko, M. Y., and Rosen, B. P. (1996) The role of arsenic-thiol interactions in metalloregulation of the ars operon. *J Biol Chem* 271, 9291-9297
32. Rensing, C., Sun, Y., Mitra, B., and Rosen, B. P. (1998) Pb(II)-translocating P-

- type ATPases. *J Biol Chem* 273, 32614-32617
33. Rensing, C., Mitra, B., and Rosen, B. P. (1997) The *zntA* gene of *Escherichia coli* encodes a Zn(II)-translocating P-type ATPase. *Proc Natl Acad Sci U S A* 94, 14326-14331
  34. Ye, J., Kandegedara, A., Martin, P., and Rosen, B. P. (2005) Crystal Structure of the *Staphylococcus aureus* pI258 CadC Cd(II)/Pb(II)/Zn(II)-Responsive Repressor. *J Bacteriol* 187, 4214-4221
  35. Cook, W. J., Kar, S. R., Taylor, K. B., and Hall, L. M. (1998) Crystal structure of the cyanobacterial metallothionein repressor SmtB: a model for metalloregulatory proteins. *J Mol Biol* 275, 337-346
  36. Aravind, L., Anantharaman, V., Balaji, S., Babu, M. M., and Iyer, L. M. (2005) The many faces of the helix-turn-helix domain: transcription regulation and beyond. *FEMS Microbiol Rev* 29, 231-262
  37. Clark, K. L., Halay, E. D., Lai, E., and Burley, S. K. (1993) Co-crystal structure of the HNF-3/fork head DNA-recognition motif resembles histone H5. *Nature* 364, 412-420
  38. Brennan, R. G. (1993) The winged-helix DNA-binding motif: another helix-turn-helix takeoff. *Cell* 74, 773-776
  39. Endo, G., and Silver, S. (1995) CadC, the transcriptional regulatory protein of the cadmium resistance system of *Staphylococcus aureus* plasmid pI258. *J Bacteriol* 177, 4437-4441
  40. Shi, W., Wu, J., and Rosen, B. P. (1994) Identification of a putative metal binding site in a new family of metalloregulatory proteins. *J Biol Chem* 269, 19826-19829
  41. Pace, C. N., Vajdos, F., Fee, L., Grimsley, G., and Gray, T. (1995) How to measure and predict the molar absorption coefficient of a protein. *Protein Sci* 4, 2411-2423
  42. Guo, J., and Giedroc, D. P. (1997) Zinc site redesign in T4 gene 32 protein: structure and stability of cobalt(II) complexes formed by wild-type and metal ligand substitution mutants. *Biochemistry* 36, 730-742
  43. Nucifora, G., Chu, L., Misra, T. K., and Silver, S. (1989) Cadmium resistance from *Staphylococcus aureus* plasmid pI258 *cadA* gene results from a cadmium-efflux ATPase. *Proc Natl Acad Sci U S A* 86, 3544-3548

44. Payne, J. C. t. H., M.A.; Godwin, H.A.; (1999) Lead fingers: Pb<sup>2+</sup> binding to structural zinc-binding domains determined directly by monitoring lead-thiolate charge-transfer bands. *J. Am. Chem. Soc* 121, 6850-6855
45. Martell, A. E., and Smith R. M. (1974-1989) *Critical Stability Constants*, Plenum Press, New York
46. Nasir, M. S., Fahrni, C. J., Suhy, D. A., Kolodsick, K. J., Singer, C. P., and O'Halloran, T. V. (1999) The chemical cell biology of zinc: structure and intracellular fluorescence of a zinc-quinolinesulfonamide complex. *J Biol Inorg Chem* 4, 775-783
47. Hemmingsen, L., Bauer, R., Bjerrum, M. J., Zeppezauer, M., Adolph, H. W., Formicka, G., and Cedergren-Zeppezauer, E. (1995) Cd-substituted horse liver alcohol dehydrogenase: catalytic site metal coordination geometry and protein conformation. *Biochemistry* 34, 7145-7153
48. Frauenfelder, H., Steffen R. M. (1965) *Alpha, Beta and Gamma Ray Spectroscopy*, North-Holland, Amsterdam
49. Hemmingsen, L., Sas, K. N., and Danielsen, E. (2004) Biological applications of perturbed angular correlations of gamma-ray spectroscopy. *Chem Rev* 104, 4027-4062
50. Pountney, D. L., Tiwari, R. P., and Egan, J. B. (1997) Metal- and DNA-binding properties and mutational analysis of the transcription activating factor, B, of coliphage 186: a prokaryotic C4 zinc-finger protein. *Protein Sci* 6, 892-902
51. Henehan, C. J., Pountney, D. L., Zerbe, O., and Vasak, M. (1993) Identification of cysteine ligands in metalloproteins using optical and NMR spectroscopy: cadmium-substituted rubredoxin as a model [Cd(CysS)<sub>4</sub>]<sup>2-</sup> center. *Protein Sci* 2, 1756-1764
52. Claudio, E. S., Magyar, J.S., Godwin, H.A. (2003) Chapter 1: fundamental coordination chemistry, environmental chemistry, and biochemistry of lead(II), *Prog. Inorg. Chem* 51, 1-144
53. Hemmingsen, L., Olsen, L., Antony, J., and Sauer, S. P. (2004) First principle calculations of (113)Cd chemical shifts for proteins and model systems. *J Biol Inorg Chem* 9, 591-599
54. Bauer, R. J., S. J.; Schmidt-Nielsen. B (1988) The angular overlap model applied to the calculation of nuclear quadrupole interactions. Derivation of partial nuclear

- quadrupole interaction parameters for biological relevant ligands in cadmium complexes. *Hyperfine Interactions* 39, 203-234
55. Hemmingsen, L., Bauer, R., Bjerrum, M. J., Schwarz, K., Blaha, P., and Andersen, P. (1999) Structure, chemical bonding, and nuclear quadrupole interactions of beta-Cd(OH)<sub>2</sub>: experiment and first principles calculations. *Inorg Chem* 38, 2860-2867
  56. Matzapetakis, M., Farrer, B. T., Weng, T. C., Hemmingsen, L., Penner-Hahn, J. E., and Pecoraro, V. L. (2002) Comparison of the binding of cadmium(II), mercury(II), and arsenic(III) to the de novo designed peptides TRI L12C and TRI L16C. *J Am Chem Soc* 124, 8042-8054
  57. Rother, D., Mattes, R., and Altenbuchner, J. (1999) Purification and characterization of MerR, the regulator of the broad-spectrum mercury resistance genes in *Streptomyces lividans* 1326. *Mol Gen Genet* 262, 154-162
  58. Kolodziej, A. F., Tan, T., and Koshland, D. E., Jr. (1996) Producing positive, negative, and no cooperativity by mutations at a single residue located at the subunit interface in the aspartate receptor of *Salmonella typhimurium*. *Biochemistry* 35, 14782-14792
  59. Anderson, A. C., O'Neil, R. H., DeLano, W. L., and Stroud, R. M. (1999) The structural mechanism for half-the-sites reactivity in an enzyme, thymidylate synthase, involves a relay of changes between subunits. *Biochemistry* 38, 13829-13836
  60. Biemann, H. P., and Koshland, D. E., Jr. (1994) Aspartate receptors of *Escherichia coli* and *Salmonella typhimurium* bind ligand with negative and half-of-the-sites cooperativity. *Biochemistry* 33, 629-634
  61. Helmann, J. D., Ballard, B. T., and Walsh, C. T. (1990) The MerR metalloregulatory protein binds mercuric ion as a tricoordinate, metal-bridged dimer. *Science* 247, 946-948
  62. Ansari, A. Z., Chael, M. L., and O'Halloran, T. V. (1992) Allosteric underwinding of DNA is a critical step in positive control of transcription by Hg-MerR. *Nature* 355, 87-89
  63. Sun, Y., Wong, M. D., and Rosen, B. P. (2002) Both metal binding sites in the homodimer are required for metalloregulation by the CadC repressor. *Mol Microbiol* 44, 1323-1329
  64. Apuy, J. L., Busenlehner, L. S., Russell, D. H., and Giedroc, D. P. (2004)

- Ratiometric pulsed alkylation mass spectrometry as a probe of thiolate reactivity in different metalloderivatives of *Staphylococcus aureus* pI258 CadC. *Biochemistry* 43, 3824-3834
65. Beard, S. J., Hashim, R., Membrillo-Hernandez, J., Hughes, M. N., and Poole, R. K. (1997) Zinc(II) tolerance in *Escherichia coli* K-12: evidence that the zntA gene (o732) encodes a cation transport ATPase. *Mol Microbiol* 25, 883-891
  66. Binet, M. R., and Poole, R. K. (2000) Cd(II), Pb(II) and Zn(II) ions regulate expression of the metal-transporting P-type ATPase ZntA in *Escherichia coli*. *FEBS Lett* 473, 67-70
  67. Brocklehurst, K. R., Hobman, J. L., Lawley, B., Blank, L., Marshall, S. J., Brown, N. L., and Morby, A. P. (1999) ZntR is a Zn(II)-responsive MerR-like transcriptional regulator of zntA in *Escherichia coli*. *Mol Microbiol* 31, 893-902
  68. Yoon, K. P., Misra, T. K., and Silver, S. (1991) Regulation of the cadA cadmium resistance determinant of *Staphylococcus aureus* plasmid pI258. *J Bacteriol* 173, 7643-7649
  69. Coombs, J. M., and Barkay, T. (2004) Molecular evidence for the evolution of metal homeostasis genes by lateral gene transfer in bacteria from the deep terrestrial subsurface. *Appl Environ Microbiol* 70, 1698-1707
  70. Borodina, I., Krabben, P., and Nielsen, J. (2005) Genome-scale analysis of *Streptomyces coelicolor* A3(2) metabolism. *Genome Res* 15, 820-829
  71. Bentley, S. D., Chater, K. F., Cerdeno-Tarraga, A. M., Challis, G. L., Thomson, N. R., James, K. D., Harris, D. E., Quail, M. A., Kieser, H., Harper, D., Bateman, A., Brown, S., Chandra, G., Chen, C. W., Collins, M., Cronin, A., Fraser, A., Goble, A., Hidalgo, J., Hornsby, T., Howarth, S., Huang, C. H., Kieser, T., Larke, L., Murphy, L., Oliver, K., O'Neil, S., Rabinowitsch, E., Rajandream, M. A., Rutherford, K., Rutter, S., Seeger, K., Saunders, D., Sharp, S., Squares, R., Squares, S., Taylor, K., Warren, T., Wietzorrek, A., Woodward, J., Barrell, B. G., Parkhill, J., and Hopwood, D. A. (2002) Complete genome sequence of the model actinomycete *Streptomyces coelicolor* A3(2). *Nature* 417, 141-147
  72. Studholme, D. J., Bentley, S. D., and Kormanec, J. (2004) Bioinformatic identification of novel regulatory DNA sequence motifs in *Streptomyces coelicolor*. *BMC Microbiol* 4, 14
  73. Karoonuthaisiri, N., Weaver, D., Huang, J., Cohen, S. N., and Kao, C. M. (2005) Regional organization of gene expression in *Streptomyces coelicolor*. *Gene* 353, 53-66



74. Helmann, J. D. (2002) The extracytoplasmic function (ECF) sigma factors. *Adv Microb Physiol* 46, 47-110
75. Bae, J. B., Park, J. H., Hahn, M. Y., Kim, M. S., and Roe, J. H. (2004) Redox-dependent changes in RsrA, an anti-sigma factor in *Streptomyces coelicolor*: zinc release and disulfide bond formation. *J Mol Biol* 335, 425-435
76. Persans, M. W., Nieman, K., and Salt, D. E. (2001) Functional activity and role of cation-efflux family members in Ni hyperaccumulation in *Thlaspi goesingense*. *Proc Natl Acad Sci U S A* 98, 9995-10000
77. Paulsen, I. T., and Saier, M. H., Jr. (1997) A novel family of ubiquitous heavy metal ion transport proteins. *J Membr Biol* 156, 99-103
78. Kobae, Y., Uemura, T., Sato, M. H., Ohnishi, M., Mimura, T., Nakagawa, T., and Maeshima, M. (2004) Zinc transporter of Arabidopsis thaliana AtMTP1 is localized to vacuolar membranes and implicated in zinc homeostasis. *Plant Cell Physiol* 45, 1749-1758
79. Ellis, C. D., Macdiarmid, C. W., and Eide, D. J. (2005) Heteromeric protein complexes mediate zinc transport into the secretory pathway of eukaryotic cells. *J Biol Chem*
80. Guffanti, A. A., Wei, Y., Rood, S. V., and Krulwich, T. A. (2002) An antiport mechanism for a member of the cation diffusion facilitator family: divalent cations efflux in exchange for K<sup>+</sup> and H<sup>+</sup>. *Mol Microbiol* 45, 145-153
81. Li, S., Rosen, B. P., Borges-Walmsley, M. I., and Walmsley, A. R. (2002) Evidence for cooperativity between the four binding sites of dimeric ArsD, an As(III)-responsive transcriptional regulator. *J Biol Chem* 277, 25992-26002
82. Moore, C. M., Gaballa, A., Hui, M., Ye, R. W., and Helmann, J. D. (2005) Genetic and physiological responses of *Bacillus subtilis* to metal ion stress. *Mol Microbiol* 57, 27-40
83. Liu, T., Golden, J. W., and Giedroc, D. P. (2005) A Zinc(II)/Lead(II)/Cadmium(II)-Inducible Operon from the *Cyanobacterium Anabaena* Is Regulated by AztR, an alpha3N ArsR/SmtB Metalloregulator. *Biochemistry* 44, 8673-8683

## VITA

Name: Yun Wang

Date of Birth: Oct. 20, 1981

Place of Birth: Hangzhou, Zhejiang Province, P. R. China

Address: Wen-2-Road CuiYuan-5-Qu 25(new)-3-601  
Hangzhou, 310012, Zhejiang, P.R.China

Education: Master of Science in Biochemistry,  
Texas A&M University, College Station, Texas, August, 2005  
Bachelor of Science in Biology,  
Fudan Univeristy, Shanghai, P. R. China, July, 2002